BABAR Analysis Document #1738, Version 04

Measurement of the parameters governing CP Violation in $B\overline{B}$ Mixing on the Recoil of partially reconstructed $\overline{B}^0 \to D^{*+}\ell^-\bar{\nu}_\ell$ using Kaon Tags

The *BABAR* Collaboration

July 5, 2007

Abstract

In this analysis we use the Run1-5 dataset to measure some parameters which determine CP violation in $B^0\overline{B}^0$ mixing and decay. $\overline{B}^0 \to D^{*+}\ell^-\bar{\nu}_\ell$ decays are selected by using partial reconstruction of the D^{*+} while the flavor of the un-reconstructed B is tagged from the charge of a kaon identified among its decay products. Detector related charge asymmetries are measured on data using the kaons coming from the partially reconstructed D^{*+}. The effects of Doubly Cabibbo Suppressed Decays on the tag side are also measured, along with the B^0 lifetime τ_{B^0} and the mixing frequency Δm_d. We get the results $|q/p| = x.xxx \pm y.yyy...$

A. Gaz, M. Margoni, F. Simonetto, Università & INFN - Padova

Contents

1 Introduction

Of the three types of CP-Violation possible in the $B^0\overline{B}^0$ system, CP-Violation in Mixing is the only one which is yet to be discovered.

In the usual formalism, the effective Hamiltonian which describes mixing and decay of B^0 mesons is written in terms of 2×2 hermitian matrices: $\mathbf{H} = \mathbf{M} - i/2\,\mathbf{\Gamma}$. In terms of the flavor eigenstates, B^0 and $\overline{B}^0$, the two eigenstates of the Hamiltonian, carrying mass m_L and m_H, are written as:

$$\begin{aligned} |B_L\rangle &= p|B^0\rangle + q|\overline{B}^0\rangle \\ |B_H\rangle &= p|B^0\rangle - q|\overline{B}^0\rangle. \end{aligned}$$

The quantity $|q/p|$ drives CP-Violation in Mixing, and is exactly equal to 1 in the CP-conserving scenario. Given its closeness to 1, and the fact that the quantity Γ_{12}/M_{12} is $O(m_b^2/m_t^2)$ it can be expressed, neglecting terms $O(m_b^4/m_t^4)$, as:

$$\left|\frac{q}{p}\right|^2 = \left|\sqrt{\frac{M_{12}^* - i/2\,\Gamma_{12}^*}{M_{12} - i/2\,\Gamma_{12}}}\right|^2 \simeq 1 - \Im\left(\frac{\Gamma_{12}}{M_{12}}\right) \tag{1}$$

One of the most recent theoretical calculations [1], which takes into account NLO QCD corrections, predicts:

$$|q/p| - 1 = (2.96 \pm 0.67) \times 10^{-4}$$

The interest in measuring this quantity relies on the fact that New Physics could enter the mixing amplitudes, potentially enhancing the amount of CP-violation predicted by the Standard Model by one order of magnitude (see e.g. [2]).

Therefore, measuring an amount of CP-violation in Mixing significantly higher than Standard Model predictions, would be a clear indication of new particles and phases contributing to $B^0\overline{B}^0$ Mixing.

1.1 Previous Measurements

Recent measurements on the magnitude of q/p have been performed at the B-factories and by the $D\emptyset$ Collaboration, using high momentum leptons to tag the flavor of the two B^0 mesons.

If CP is violated in Mixing, the probability of a B^0 to oscillate to a $\overline{B}^0$ is different from the probability of a $\overline{B}^0$ to oscillate to a B^0 and thus we expect to observe a different number of B^0 B^0 events with respect to $\overline{B}^0$ $\overline{B}^0$. $|q/p|$ is related to the asymmetry $\mathcal{A}_{SL}$ through:

$$\mathcal{A}_{SL} = \frac{N(B^0B^0) - N(\overline{B}^0\overline{B}^0)}{N(B^0B^0) + N(\overline{B}^0\overline{B}^0)} = \frac{N(\ell^+\ell^+) - N(\ell^-\ell^-)}{N(\ell^+\ell^+) + N(\ell^-\ell^-)} \simeq 2\left(1 - \left|\frac{q}{p}\right|\right) \tag{2}$$

The Belle [3] and *BABAR* [4] Collaborations presented a measurement based on the analysis of dilepton events. This method benefits from the high statistics achievable at the B-factories, but heavily relies on data control samples to determine detector related charge asymmetries.

The $D\emptyset$ Collaboration [5] can reach a precision comparable to the B-factories but the final result is an average on the mixing parameters of both B_d^0 and B_s^0 mesons. All the above results are summarized in table 1.

Table 1: Recent results on $|q/p|$ or $\mathcal{A}_{SL}$. The first quoted error is the statistical one, while the second is the systematic.

Analysys	Luminosity	Result
Belle dileptons	78 fb^{-1}	$\mathcal{A}_{SL} = (-1.1 \pm 7.9 \pm 9.5) \times 10^{-3}$
BABAR dileptons	210 fb^{-1}	$\lvert q/p \rvert - 1 = (-0.8 \pm 2.7 \pm 1.9) \times 10^{-3}$
$D\emptyset$ $(\mu\mu)$	1.0 fb^{-1}	$\mathcal{A}_{SL} = (-9 \pm 4 \pm 3) \times 10^{-3}$
BABAR PR $D^*\ell\nu$ leptonic tag	200 fb^{-1}	$\lvert q/p \rvert - 1 = (6.5 \pm 3.4 \pm 2.0) \times 10^{-3}$

A novel approach to the measurement of $|q/p|$ has been carried out in *BABAR*, by taking advantage of the large sample of partially reconstructed $B^0 \to D^{*-}\ell^+\nu$ events. Here the flavor of one B meson is determined by the charge of the lepton and the flavor of the other B can be measured either by searching for one more high momentum lepton or for a charged kaon.

The lepton tag has been used to get the preliminary result [6] presented at ICHEP06. Though based on a selected sample (one partially reconstructed $\overline{B}^0 \to D^{*+}\ell^-\bar{\nu}_\ell$ decay versus inclusive lepton) several times smaller than the one used in the dilepton analysis, the statistical error is still competitive with that result.

In this BAD, we will use the same reconstruction technique, exploiting the kaon tag in order to increase the statistical significance. Besides the higher mistag rate, the kaon tag analysis differs from the lepton tag for the presence of Doubly Cabibbo Suppressed decays, which will be measured in this analysis, and for the presence of significantly higher detector related charge asymmetries.

The latter is a crucial issue; charge asymmetries will be measured on data, exploiting the technique described in section 4.

Finally, the large sample of $B^0\overline{B}^0$ events studied in our analysis allows us to perform a measurement of the B^0 lifetime τ_{B^0} and the mixing frequency Δm_d.

2 Theoretical B decay rates

Throughout this analysis we will always assume that CPT is conserved.

The two B mesons produced by the decay of the $\Upsilon(4S)$ evolve coherently until one of them decays. Throughout this note, the B which undergoes the semileponic decay $B^0 \to D^{*-}\ell^+\nu$ will be referred to as B_{rec} while the other (not reconstructed) B will be called B_{tag}.

In our analysis, the flavor of the latter is inferred through the charge of a kaon originating from its decay, either *directly* (e.g. $B \to KX$, or *indirectly*, through an intermediate charmed meson $B \to D^{(*)}Y$, $D^{(*)} \to KZ$). A K^+ tags a B^0 while a K^- is likely to come from a $\overline{B}^0$.

Uncorrect assignments could arise from wrong particle identification, (doubly) Cabibbo suppressed Decays of a charm meson (e.g. $\overline{B}^0 \to \bar{D}^0X$, $\bar{D}^0 \to K^+K^-, \pi^-K^+, ...$) or doubly Cabibbo suppressed decays of the B^0 meson, as depicted in fig. 1. In the following, we will focus on B-meson Doubly Cabibbo Suppressed (DCS) decays.

The effects of the presence of DCS decays in the tag side have been studied in [7] and are taken into account in our analysis.

Having defined $\Delta t = t_{rec} - t_{tag}$, where t_{rec} (t_{tag}) is the decay time of B_{rec} (B_{tag}), the B-meson decay rate can be written as [8]:

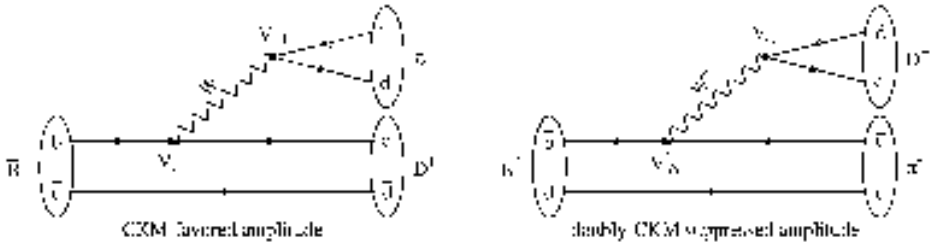

Figure 1: Example of intefering amplitudes for the $D^+\pi^-$ final state.

$$\frac{dN}{dt} \propto e^{-\Gamma|\Delta t|}\Big[\frac{1}{2}(|a_+|^2+|a_-|^2)\cosh(\Delta\Gamma\Delta t/2)+\frac{1}{2}(|a_+|^2-|a_-|^2)\cos(\Delta m_d\Delta t)- \\ -\Re(a_+^* a_-)\sinh(\Delta\Gamma\Delta t/2)+\Im(a_+^* a_-)\sin(\Delta m_d\Delta t)\Big] \tag{3}$$

where:

$$\begin{aligned} a_+ &= -\mathcal{A}_{tag}\overline{\mathcal{A}}_{rec}-\overline{\mathcal{A}}_{tag}\mathcal{A}_{rec} \\ a_- &= \frac{p}{q}\mathcal{A}_{tag}\mathcal{A}_{rec}-\frac{q}{p}\overline{\mathcal{A}}_{tag}\overline{\mathcal{A}}_{rec} \end{aligned} \tag{4}$$

Given the smallness of the difference of decay widths of the light and heavy eigenstates $\Delta\Gamma$, we will neglect the $\Re(a_+^* a_-)$ term from now on. $\mathcal{A}$ and $\overline{\mathcal{A}}$ are the amplitudes for a B^0 and $\overline{B}^0$ decay respectively. In our case, $\mathcal{A}_{rec} = \mathcal{A}(B^0 \to D^{*-}\ell^+\nu) = \overline{\mathcal{A}}_{rec}$ and $\mathcal{A}_{tag}$ is the sum of all the amplitudes with one (or more) charged kaons in the final state. Without taking into account experimental effects for now, DCS decays would cause a fraction of B^0 to be wrongly tagged as $\overline{B}^0$ and vice versa in a time integrated analysis. The study of the time dependent asymmetry permits to disentangle the effects due to DCS decays from those induced by mixing.

We define $\mathcal{A}_{CF}$ the amplitude for a B^0 to undergo a Cabibbo favored (CF) decay and thus be correctly tagged as a B^0 and $\mathcal{A}_{DCS}$ the amplitude of a B^0 decaying into a DCS final state and thus being tagged as a $\overline{B}^0$. We accordingly define $\overline{\mathcal{A}}_{CF}$ and $\overline{\mathcal{A}}_{DCS}$ for $\overline{B}^0$ CF and DCS decays respectively. Taking $r' = \left|\overline{\mathcal{A}}_{DCS}/\mathcal{A}_{CF}\right|$, the modulus of the ratio between DCS and CF amplitudes, the following relations hold:

$$\begin{aligned} \mathcal{A}_{CF} &= \overline{\mathcal{A}}_{CF} = |\mathcal{A}_{CF}|\, e^{i\delta_c} \\ \overline{\mathcal{A}}_{DCS} &= r'\,|\mathcal{A}_{CF}|\, e^{i\delta_u} e^{i\gamma} \\ \mathcal{A}_{DCS} &= r'\,|\mathcal{A}_{CF}|\, e^{i\delta_u} e^{-i\gamma} \end{aligned} \tag{5}$$

where δ_c and δ_u are the strong phases of the CF $b \to c$ and the DCS $b \to u$ transitions respectively, while γ is the relative weak phase between the two processes. Taking the weak phase of the ratio of the mixing parameters as -2β:

$$\frac{q}{p} = \left|\frac{q}{p}\right| e^{-2i\beta} \tag{6}$$

we can finally define the two parameters governing the DCS decays effects on the tag side:

$$b = 2r' \sin(2\beta+\gamma)\cos\delta'$$
$$c = -2r' \cos(2\beta+\gamma)\sin\delta' \tag{7}$$

where $\delta' = \delta_u - \delta_c$.

We are now ready to define our signal pdf's. The four possible final states are distinguished by the two indexes s_t and s_m; s_t is equal to 1 (-1) when B_{tag} is a B^0 ($\overline{B}^0$), and s_m is 1 (-1) in case of an unmixed (mixed) state. This is summarized in table 2.

Table 2: Value of s_t and s_m indexes for the four possible signal final states.

B_{rec} is a	B_{tag} is a	s_t	s_m
B^0	B^0	1	-1
$\overline{B}^0$	B^0	1	1
B^0	$\overline{B}^0$	-1	1
$\overline{B}^0$	$\overline{B}^0$	-1	-1

The signal pdf's are then the following:

$$s_t = 1,\ s_m = -1:$$
$$\mathcal{F}(\Delta t) = \frac{\Gamma}{2(1+r'^2)} e^{-\Gamma|\Delta t|}\left|\frac{p}{q}\right|^2 \Bigg[\left(1+\left|\frac{q}{p}\right|^2 r'^2\right)\cosh(\Delta\Gamma\Delta t/2) - \tag{8}$$
$$- \left(1-\left|\frac{q}{p}\right|^2 r'^2\right)\cos(\Delta m_d \Delta t) + \left|\frac{q}{p}\right|(b+c)\sin(\Delta m_d\Delta t)\Bigg]$$

$$s_t = 1,\ s_m = 1:$$
$$\mathcal{F}(\Delta t) = \frac{\Gamma}{2(1+r'^2)} e^{-\Gamma|\Delta t|}\Bigg[\left(1+\left|\frac{q}{p}\right|^2 r'^2\right)\cosh(\Delta\Gamma\Delta t/2) + \tag{9}$$
$$+ \left(1-\left|\frac{q}{p}\right|^2 r'^2\right)\cos(\Delta m_d \Delta t) - \left|\frac{q}{p}\right|(b+c)\sin(\Delta m_d\Delta t)\Bigg]$$

$$s_t = -1,\ s_m = 1:$$
$$\mathcal{F}(\Delta t) = \frac{\Gamma}{2(1+r'^2)} e^{-\Gamma|\Delta t|}\Bigg[\left(1+\left|\frac{p}{q}\right|^2 r'^2\right)\cosh(\Delta\Gamma\Delta t/2) + \tag{10}$$
$$+ \left(1-\left|\frac{p}{q}\right|^2 r'^2\right)\cos(\Delta m_d \Delta t) + \left|\frac{p}{q}\right|(b-c)\sin(\Delta m_d\Delta t)\Bigg]$$

$$s_t = -1,\ s_m = -1:$$
$$\mathcal{F}(\Delta t) = \frac{\Gamma}{2(1+r'^2)} e^{-\Gamma|\Delta t|}\left|\frac{q}{p}\right|^2 \Bigg[\left(1+\left|\frac{p}{q}\right|^2 r'^2\right)\cosh(\Delta\Gamma\Delta t/2) - \tag{11}$$
$$- \left(1-\left|\frac{p}{q}\right|^2 r'^2\right)\cos(\Delta m_d \Delta t) - \left|\frac{p}{q}\right|(b-c)\sin(\Delta m_d\Delta t)\Bigg]$$

Figures 2 and 3 show the effect of the parameters ($|q/p|$ - 1) and b and c being different from 0 for mixed and unmixed $s_t = +1$ events.

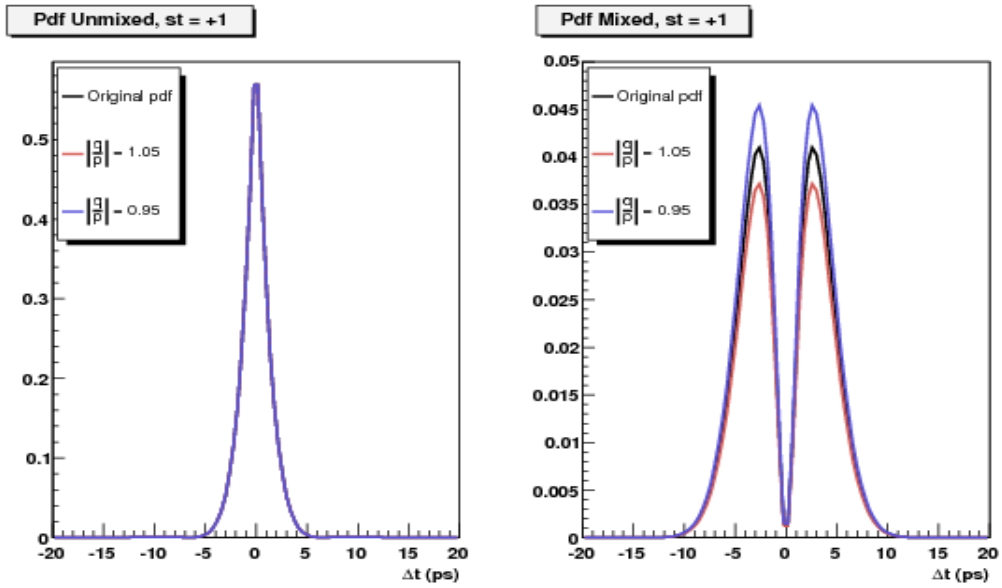

Figure 2: Δt pdf's with $|q/p| = 1$ (black curve), 1.05 (red) and 0.95 (blue) for $s_t = +1$ unmixed (left plot) and mixed (right) events. The values of $|q/p|$ plotted are un-realistically large and are used here for the only purpose of highlighting the effects of $|q/p| \neq 1$ on the mixed and unmixed pdf's.

3 Data Sets and Sample Selection

The current analysis is based on `analysis-31, 32` releases and includes all Run1-Run5 datasets. Root-uples have been produced over the R18 `InclSemiLept` skim, which pre-selects events with at least one partially reconstructed $\overline{B}^0 \to D^{*+}\ell^-\bar{\nu}_\ell$ candidate.

The full integrated luminosity of on-peak data used is equal to 348.1 fb^{-1}, equivalent to about 383 million $B\overline{B}$ pairs. Details on data samples are summarized in Table 3.

Table 3: Integrated luminosities of data samples

Data set	off-peak (fb^{-1})	on-peak (fb^{-1})	$N_{B\overline{B}}$ (10^6)
Run1	2.5	20.3	22.0
Run2	6.9	60.7	67.0
Run3	2.5	32.3	35.7
Run4	9.9	100.9	110.5
Run5	14.1	134.0	147.5
Total	35.9	348.1	382.7

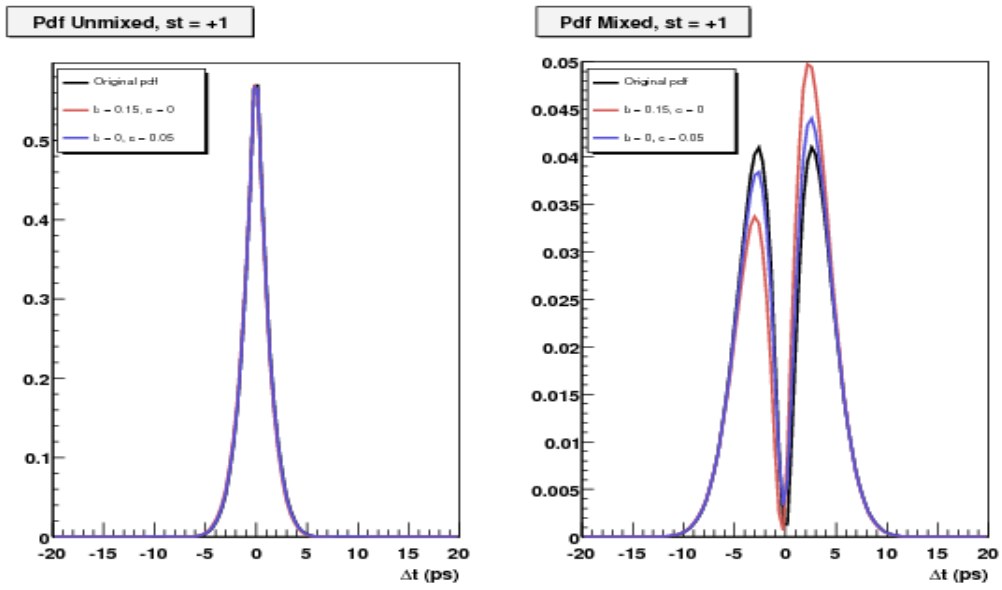

Figure 3: Δt pdf's for the Doubly Cabibbo Suppressed parameters being $(b, c) = (0, 0)$ (black), $(b, c) = (0.15, 0)$ (red) and $(b, c) = (0, 0.05)$ (blue). Again, the values of b and c used for these plots are much larger than expectations and are used here just to displaying the distortions on the pdf's caused by these effective parameters being different from 0.

This analysis has been set up using mainly the available SP generic $B\overline{B}$ Monte Carlo simulation. Again, simulated events are requested to pass the `InclSemiLept` skim criteria; the number of $B\overline{B}$ events is about 3 times larger than the one expected on data. Details can be found in Table 4.

Table 4: Number of Generic Monte Carlo generated events

Data set	$B^0\overline{B}^0$ (10^6)	$B^+B^-(10^6)$
Run1	35.8	35.6
Run2	103.5	102.9
Run3	50.6	46.1
Run4	167.1	168.3
Run5	166.4	168.8
Total	523.4	521.7

3.1 Selection of partially reconstructed $\overline{B}^0 \to D^{*+}\ell^-\bar{\nu}_\ell$ events

The technique for selecting partially reconstructed $\overline{B}^0 \to D^{*+}\ell^-\bar{\nu}_\ell$ decays is thoroughly described in [9].

We reconstruct the $\overline{B}^0 \to D^{*+}\ell^-\bar{\nu}_\ell$ (charge conjugation is always implied in this section) decay using only the information coming from the ℓ^- and the charged pion originating from the $D^{*-} \to$

$\bar{D}^0\pi^-$ decay which, due to the kinematics of the decay, will be referred to as π_{soft} hereafter.

The momenta of the two particles are requested to satisfy the following cuts: $0.06 < |\vec{p}_{\pi_{soft}}| < 0.20$ GeV/c and $1.40 < |\vec{p}_\ell| < 2.30$ GeV/c. The π_{soft} and ℓ are selected from the `ChargedTracks` list, and the PID selectors used for the lepton are `PIDLHElectrons` and `muNNLoose`.

The vertex of the ℓ, π_{soft} pair is computed constraining the x-y coordinates to the *beamspot* position (the width of the *beamspot* is enlarged to 50 μm, to account for the B-motion in the transverse plane). The momenta of the two particles and their probability to originate from a common vertex are combined in a Likelihood Ratio variable χ, which can vary from 0 (background like) and 1 (signal like). Events with $\chi < 0.3$ are rejected. Figure 4 shows the plot of the difference between the measured and the true z coordinate for B_{rec} mesons and the relative pull distribution at the end of our selection.

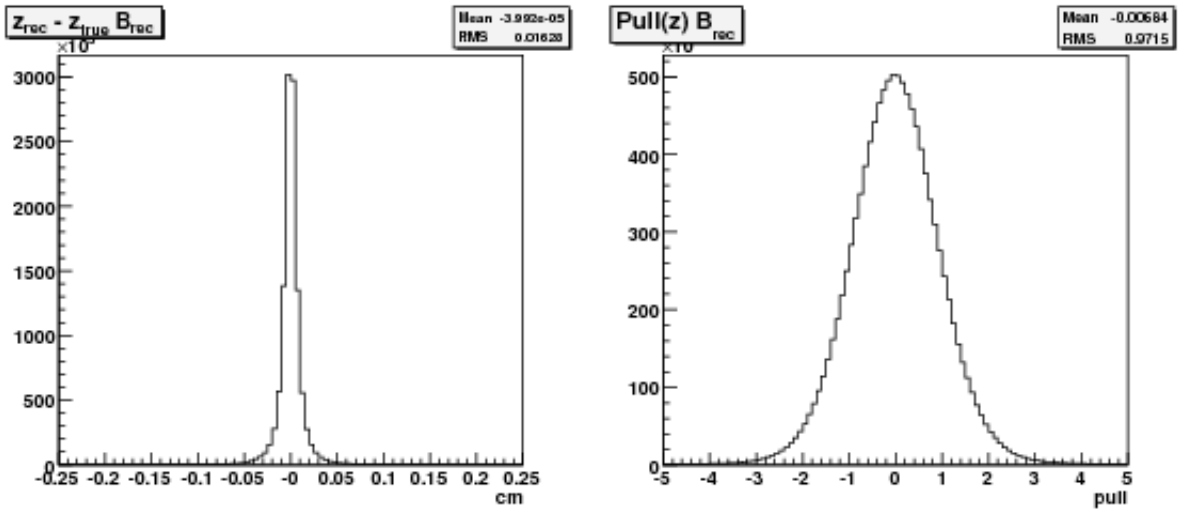

Figure 4: Measured z - true z (left plot) and pull (right) distributions for B_{rec} mesons.

Given the limited phase-space of the $D^{*-} \to \bar{D}^0\pi^-$ decay, the flight direction of the π_{soft} is roughly coincident with the one of the D^*, and the magnitude of the D^* momentum can be computed with good approximation as a (polynomial) function of the π_{soft} momentum.

Neglecting the small momentum of the candidate B^0 meson in the $\Upsilon(4S)$ rest frame, we compute the quantity:

$$m_\nu^2 = (\mathcal{P}_{B^0} - \mathcal{P}_{D^*} - \mathcal{P}_\ell)^2, \tag{12}$$

where $\mathcal{P}_x$ indicates the four-momentum of particle x.

The squared neutrino invariant mass, m_ν^2, peaks at 0 GeV/c^2 for signal events, while for background it is roughly uniformly distributed between -10 and +2.5 GeV/c^2. We define a *MassBand* region, $-2.5 < m_\nu^2 < +2.5$ GeV/c^2, which includes most of the signal and a *SideBand* region, $m_\nu^2 < -2.5$ GeV/c^2, dominated by continuum and combinatorial background. More details on the selection and the composition of our sample can be found in [9].

Figure 5 shows the m_ν^2 distribution for events with at least one tag kaon candidate. The plot has been made using the whole Run1-5 data and MC dataset; continuum events are taken from off-resonance data and are scaled with the appropriate luminosity factor with respect to $B\overline{B}$ Monte

Carlo. The resulting MC + off-resonance distribution has been normalized to on-resonance data in the region $-8 < m_\nu^2 < -4\,GeV^2/c^4$.

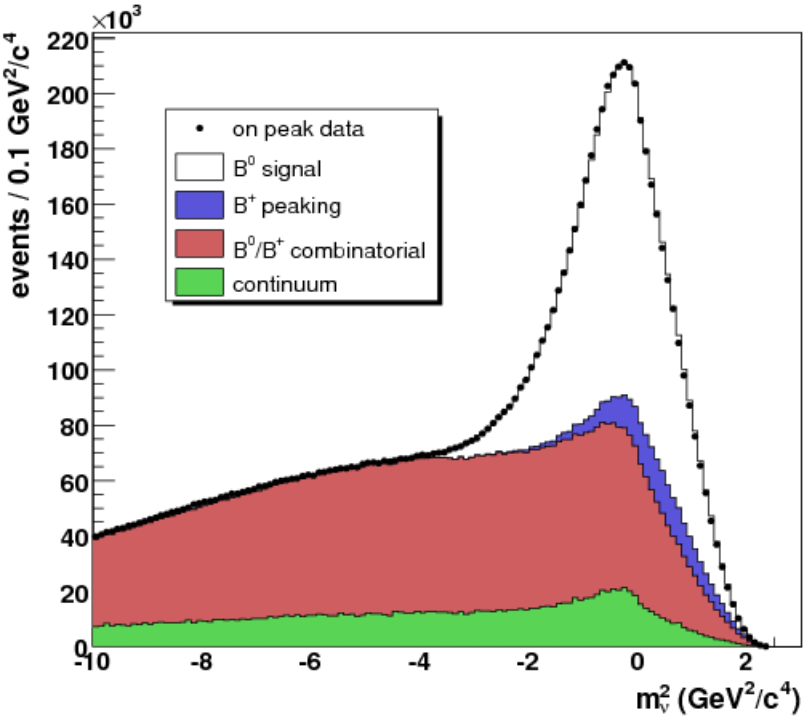

Figure 5: m_ν^2 distribution for data and the different components of Monte Carlo in events with at least one tag kaon candidate. Continuum events are taken from off-resonance data. No corrections have been applied, besides taking into account the appropriate luminosity factors and normalizing MC + off-resonance to on-resonance data in the region $-8 < m_\nu^2 < -4\,GeV^2/c^4$.

3.2 Selection of charged kaons

The sign of a charged kaon identified as a decay product of the B_{tag} is used to determine the flavor of the B_{tag} itself. The z coordinate of the B_{tag} decay vertex is computed by extrapolating the K track to the x, y coordinates of the *beamspot*. The extrapolation is performed assuming that the particle which gave that track has the pion mass; this causes a dependence of some of the parameters entering the resolution model on the kaon momentum, as discussed in section 5. In figure 6 we show the dependence of the width of the narrow component in the resolution function for B_{tag} signal events for genuine $K^\pm$ and pions faking kaons.

Figure 7 shows the distribution of the difference of the measured z coordinate and the true one along with its pull for B_{tag} mesons.

The separation between the two B vertices Δz is defined as $\Delta z = z(B_{rec}) - z(B_{tag})$ and its uncertainty $\sigma(\Delta z)$ is computed by propagating the uncertainties on the determinations of the two vertices.

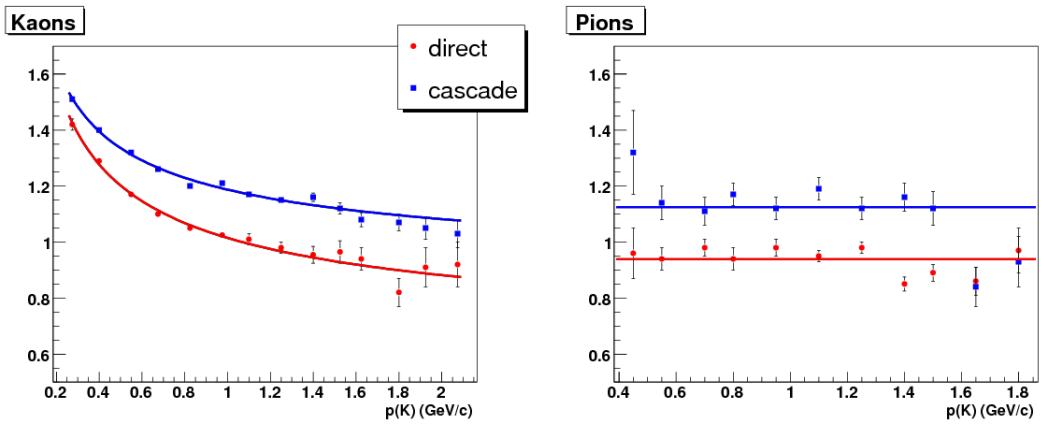

Figure 6: Pull of the narrow component in the resolution model for signal B_{tag} events for true kaons (left) and pions (right). Direct decays (red circles) are shown separately from cascades (blue squares).

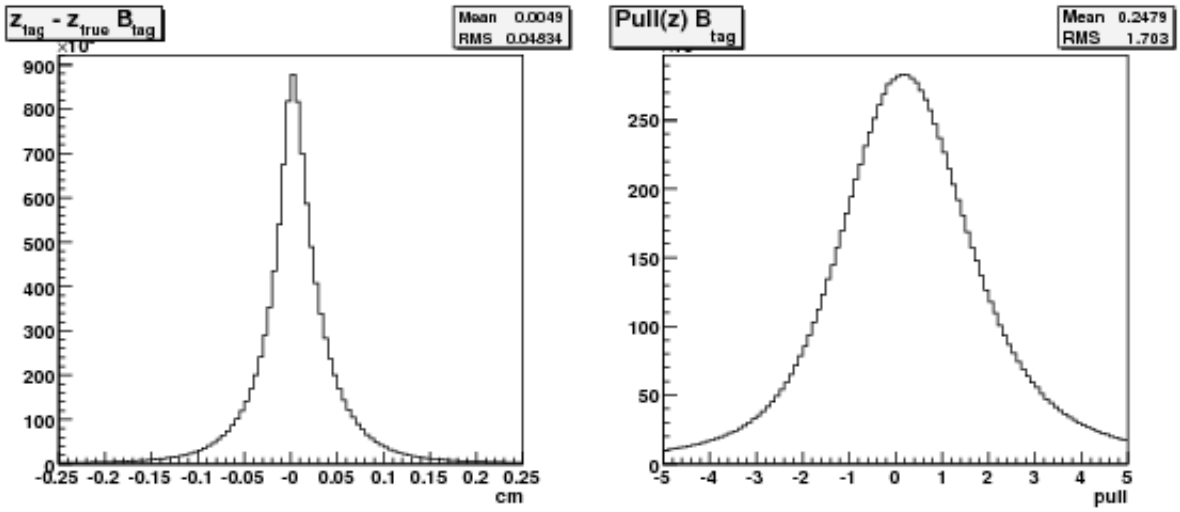

Figure 7: Measured z - true z (left plot) and pull (right) distributions for B_{tag} mesons.

$K^{\pm}$ tracks are selected from `ChargedTracks` and are requested to pass the `LooseKaonMicro` PID selector. Furthermore, we request $|\Delta z| < 0.3$ cm and $\sigma(\Delta z) < 0.05$ cm.

The proper time difference Δt between the decays of B_{rec} and B_{tag} is computed in the *boost approximation*: $\Delta t = \Delta z / \beta\gamma c$.

4 Measurement Technique

In case of CP Violation in $B^0\overline{B}^0$ Mixing, the probability of oscillation of a B^0 state into a $\overline{B}^0$ would be different from the probability of the inverse process. Therefore the number of B^0B^0 decays, integrated over the decay times, would be different from the number of $\overline{B}^0\overline{B}^0$ events.

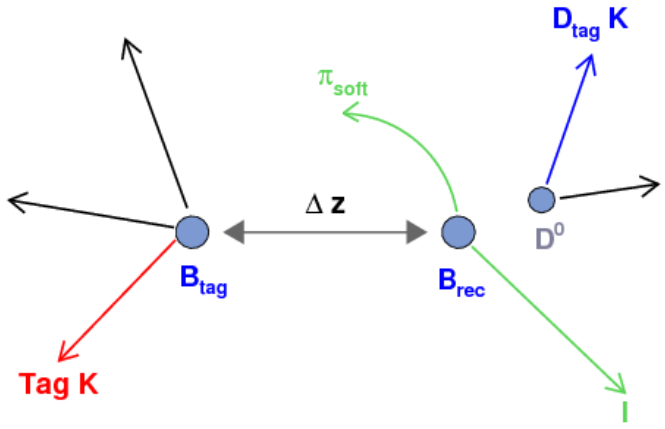

Figure 8: Schematic drawing of a possible signal event

Figure 8 shows a schematic picture of a possible signal event. B_{rec} is partially reconstructed by using only the information coming from the π_{soft}, ℓ pair.

Charged kaons may originate from the decay of the unreconsctructed B_{tag} and are used to tag its flavor; we will call them B_{tag} *kaons*. Kaons could also come from the decay of the D^0 on the B_{rec} side (D_{tag} *kaons*); most of them have the same charge of the lepton coming from B_{rec}. The small fraction of D_{tag} kaons having opposite charge with respect to the lepton originate from (doubly) Cabibbo Suppressed decays ($D^0 \to K^+K^-, K^+\pi^-, ...$), mistags ($D^0 \to K^-\pi^+X, \pi^+ \to \text{fake}K^+$).

Given the difference between D^0 and B^0 lifetimes and the fact that the B_{tag} decay vertex is computed by using only the K track, D_{tag} and B_{tag} kaons exhibit different Δz distributions, the former being much narrower than the latter (see figure 9). Moreover, the flight direction of a D_{tag} kaon is correlated to the flight directions of B_{rec} side ℓ and π_{soft} and those correlations can be used to extract the fractions of D_{tag} kaons as a function of the angles of its trajectory with respect to the B_{rec} pair.

The presence of the D_{tag} K sample allows us to measure directly on data the detector related charge asymmetries which give a higher probability of reconstructing a B^0B^0 event rather than a $\overline{B}^0\overline{B}^0$ one. In section 4.2 some results, based on Monte Carlo studies, on this method of measuring

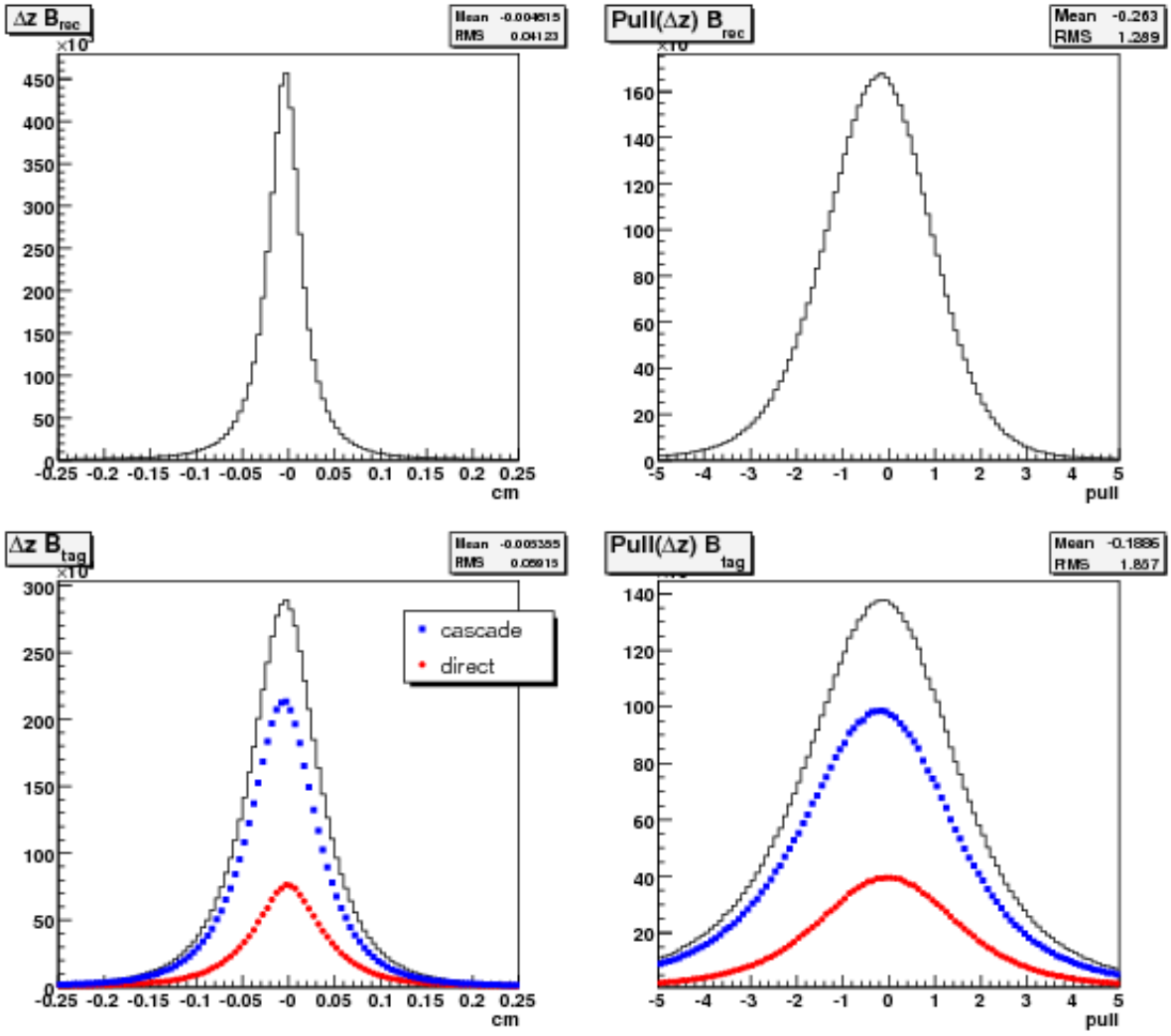

Figure 9: Δz distributions (left plots) and relative pull (right) for D_{tag} (top) and B_{tag} (bottom) events. In the computation of D_{tag} pull the true value of Δz is 0 by definition, since the kaon and the ℓ, π_{soft} pair originate from the same B meson. For the B_{tag} events, we show the contributions of direct $b \to K$ decays (red circles) and of the cascade $b \to c \to K$ decays (blue squares).

the charge asymmetries will be given, prior to the description of the whole Probability Density Function (PDF) to be used in the nominal fit.

4.1 Fitting technique

The main physics parameters, along with the ones related to detector response and resolution are fitted simultaneously in a binned Maximum Likelihood fit on the variables Δt, $\sigma(\Delta t)$. In the fit, we account explicitly for the dependence of Δt and $\sigma(\Delta t)$ on the kaon momentum $|\vec{p}_K|$.

We use 100 bins for Δt, 25 bins for $\sigma(\Delta t)$ and 5 bins for $|\vec{p}_K|$. The Likelihood value is computed at the center of each bin. Several constraints (e.g. that the fraction of mixed events should be equal to $\chi^2_d/[2(1+\chi^2_d)]$, where $\chi_d = \Delta m_d \tau_{B^0}$) are applied to the Likelihood; this is equivalent to the use of an Extended Maximum Likelihood formalism.

The fractions of *Signal*, *Combinatorial*, *Peaking* and *Continuum* are determined from a fit to the m^2_ν distribution.

The fraction of D_{tag} kaons is extracted by exploiting their correlation with the B_{rec} side ℓ flight direction. Figure 10 shows the cosine of the angle between the candidate K and the ℓ ($\cos(\theta_{K\ell})$) for signal and background B_{tag} and D_{tag} events.

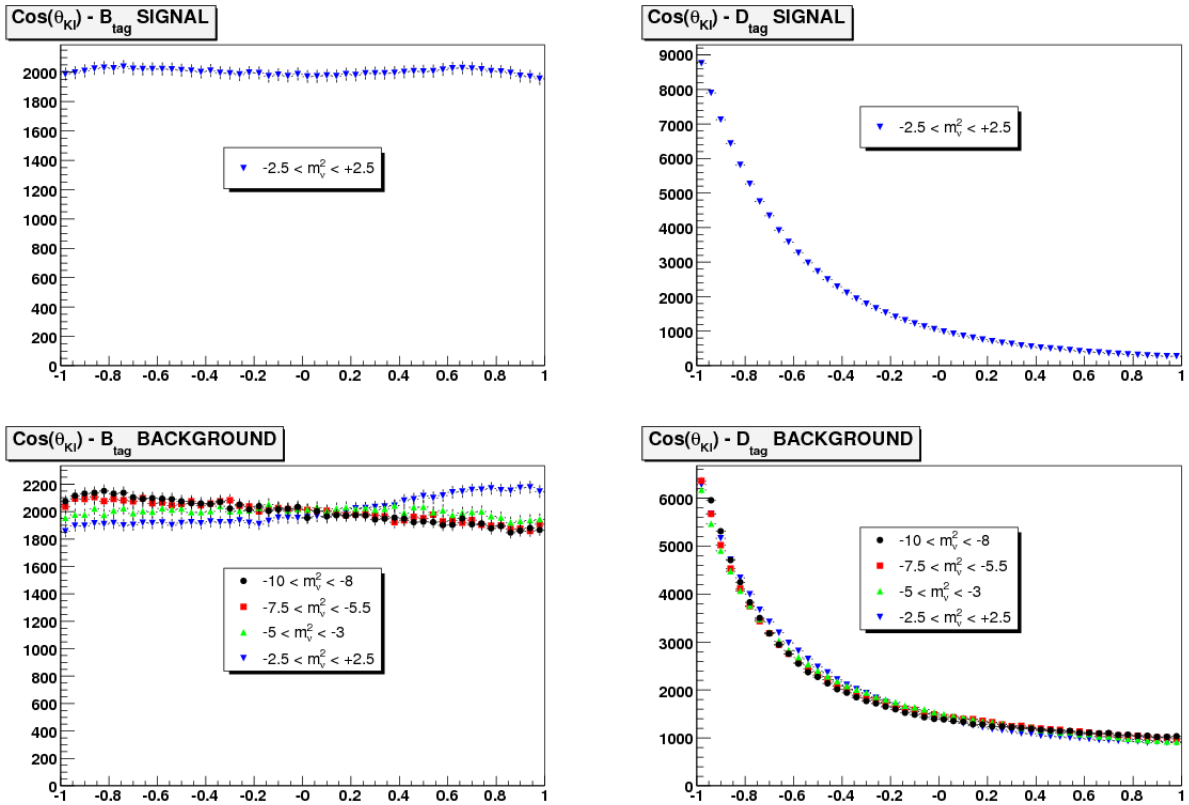

Figure 10: $\cos(\theta_{K\ell})$ for B_{tag} (left plots) and D_{tag} (right) events. Top plots show the distributions for events where the $\ell\pi_{soft}$ pair is a signal one, while bottom plots show $B^0\overline{B}^0$ combinatorial events in four different ranges of m^2_ν. All distributions have been normalized to the same arbitrary area.

As the kaon and the lepton originate from different B-mesons in B_{tag} events, their flight directions are un-correlated and thus the $\cos(\theta_{K\ell})$ distributions are roughly flat.

On the other side, for D_{tag} events, K and ℓ tracks originate from the decay of the same B meson, which has a very little momentum in the $\Upsilon(4S)$ rest frame. The kinematics of the $B^0 \to D^{*-}\ell^+\nu$, $D^{*-} \to \bar{D}^0\pi^-_{soft}$, $\bar{D}^0 \to K^+X$ decay chain is such that the angle between the kaon and the lepton is preferentially large. Figure 10 shows that $\cos(\theta_{K\ell})$ peaks towards -1 for both signal and background events and that there is a negliglible dependence on the value of m^2_ν.

The D_{tag} fraction is determined from a polynomial fit to the $\cos(\theta_{K\ell})$ distribution.

4.2 Charge Asymmetries

Detector related charge asymmetries on the B_{tag} and D_{tag} samples can be measured on generic Monte Carlo (which is generated with no physical charge asymmetry) by simply counting K^+ and K^- and using the MC truth.

The results for this test, run over Run1-4 generic $B^0\overline{B}^0$ MC, are presented in table 5, where we show the quantity:

$$A_{\ell K} = \frac{N(\ell^+K^+) - N(\ell^-K^-)}{N(\ell^+K^+) + N(\ell^-K^-)},$$

separately for K from the tag side and from the decay side. Only signal events and true kaons are considered and events where the B_{rec} lepton is identified as a muon are separated from the electron case (A_K includes also the asymmetry in the reconstruction of B_{rec}).

Table 5: Results of the test of charge asymmetries on Run1-5 generic $B^0\overline{B}^0$ MC. Only true kaons have been selected.

	Electrons	Muons
$A_{\ell K}(B_{tag})$	0.0149 ± 0.0013	0.0196 ± 0.0016
$A_{\ell K}(D_{tag})$	0.0152 ± 0.0009	0.0205 ± 0.0010

There is a very good agreement between the charge asymmetries measured in B_{tag} and D_{tag} samples for separately electrons and muons, so the method of constraining the detector related asymmetries to the ones found on the D_{tag} sample looks feasible.

As the momentum ($|\vec{p}_L|$) and the polar angle (ϑ_L) spectra are different for B_{tag} and D_{tag} kaons (see figures 11 and 12) and charge asymmetries depend on those variables, we need to check that there is not a strong dependence of the asymmetries on small variations of the spectra predicted by our Monte Carlo.

First of all we check that the charge asymmetry for B_{tag} and D_{tag} detection is the same in a given (small) range of $|\vec{p}_L|$ and ϑ_L. We divide the ($|\vec{p}_L|$, ϑ_L) 2-dimensional spectrum in 400 squared bins and for each of them (if it contains at least 50 events), compute the quantity:

$$pull(Asy) = \frac{A_{Btag} - A_{Dtag}}{\sqrt{\sigma^2(A_{Btag}) + \sigma^2(A_{Dtag})}}.$$

The result is shown in figure 13; it can be seen that, as expected, the two charge asymmetries are well compatible with each other within statistical uncertainties.

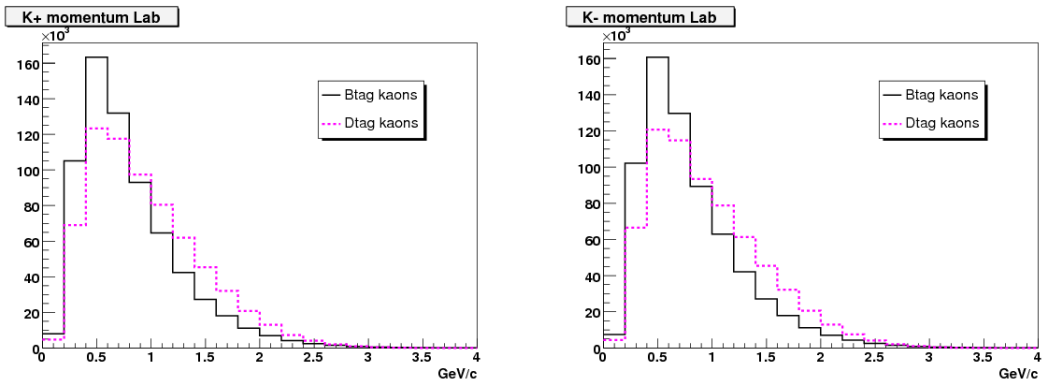

Figure 11: Distributions of B_{tag} and D_{tag} momenta in the laboratory frame, separately for K^+ (left plot) and K^- (right). D_{tag} spectra have been normalized to B_{tag} ones.

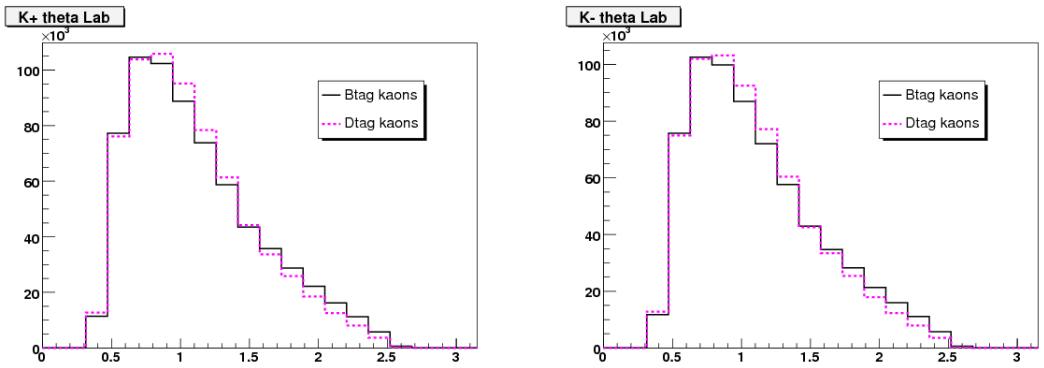

Figure 12: Distributions of B_{tag} and D_{tag} polar angles in the laboratory frame (ϑ_L), separately for K^+ (left plot) and K^- (right). D_{tag} spectra have been normalized to B_{tag} ones.

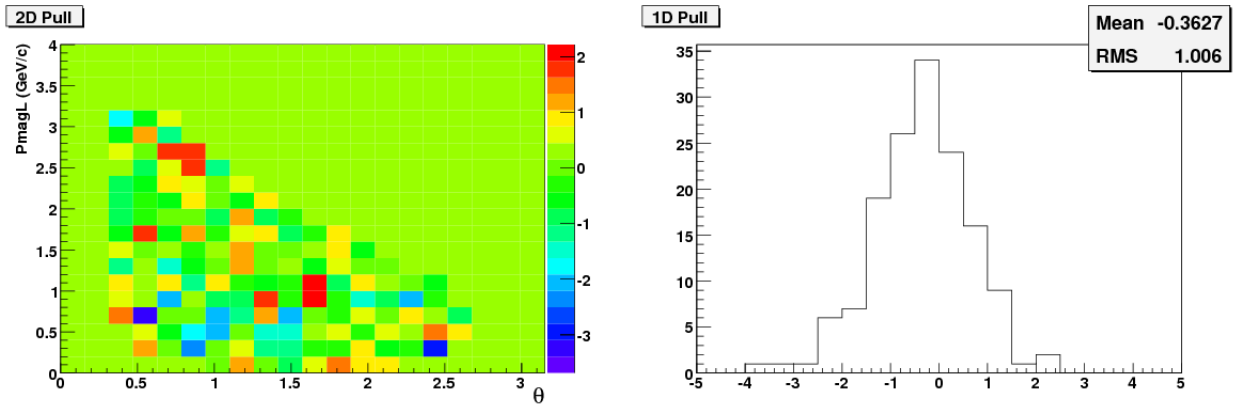

Figure 13: Distribution of *pull(Asy)* for Run1-4 generic $B^0\overline{B}^0$ Monte Carlo as a function of ($|\vec{p}_L|$, ϑ_L) (left plot). The distribution of *pull(Asy)* for bins containing at least 50 events of B_{tag} and D_{tag} kaons is shown in the right plot.

To check the dependence of charge asymmetries on the shapes of $|\vec{p}_L|$ and ϑ_L spectra, we generate a few datasets with modified spectra, according to the following procedure. To generate datasets with modified $|\vec{p}_L|$ spectra, we randomly select, from the initial sample, D_{tag} kaons with a probability:

$$prob(|\vec{p}_L|) = 0.9 + m(|\vec{p}_L| \ - 2),$$

(with $|\vec{p}_L|$ in GeV/c) and $m \in [-0.5, \ldots, +0.5]$, independently of ϑ_L and regardless of the kaon charge. We do the same generating datasets with ϑ_L spectra modified according to the probability:

$$prob(\vartheta_L) = 0.9 + m(\vartheta_L \ - 1.575),$$

and m in the same range as before. Figure 14 shows the modified $|\vec{p}_L|$ and ϑ_L spectra for the extreme cases and the unmodified shapes.

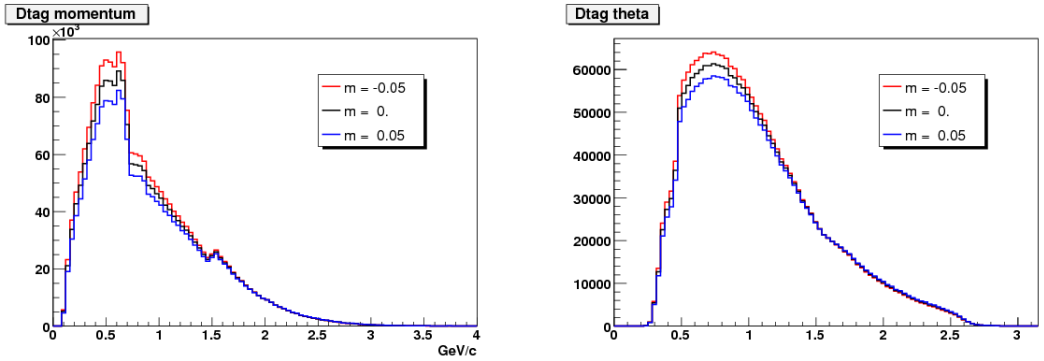

Figure 14: Modified $|\vec{p}_L|$ (left plot) and ϑ_L (right) spectra for the extreme cases ($m = \pm 0.5$) and the original shape ($m = 0$).

For each generated dataset, we compute the charge asymmetries (separately for electrons and muons). The results are reported in figure 15.

No sizable deviations appear on the modified spectra with respect to the original case. We conclude that the method of constraining detector related charge asymmetries to the ones measured on the D_{tag} sample is reliable, within the uncertainties on the Monte Carlo which are covered by our modified datasets.

5 Signal and Background description

As stated in section 4, CP violation in mixing would manifest itself giving a number of B^0B^0 events different from the one of $\overline{B}^0\overline{B}^0$.

The flavor of B_{rec} is given by the sign of the lepton: a positive (negative) lepton tags a B^0 ($\overline{B}^0$). The same happens for B_{tag} where (a part for much larger dilution effects) a positive (negative) K tags a B^0 ($\overline{B}^0$).

In this analysis we plan to fit simultaneously the following four subsamples:

- *Unmixed positive* (UP): B_{tag} kaon is a positive one and the lepton on B_{rec} side is negative (K^+, ℓ^-);
- *Unmixed negative* (UN): (K^-, ℓ^+);

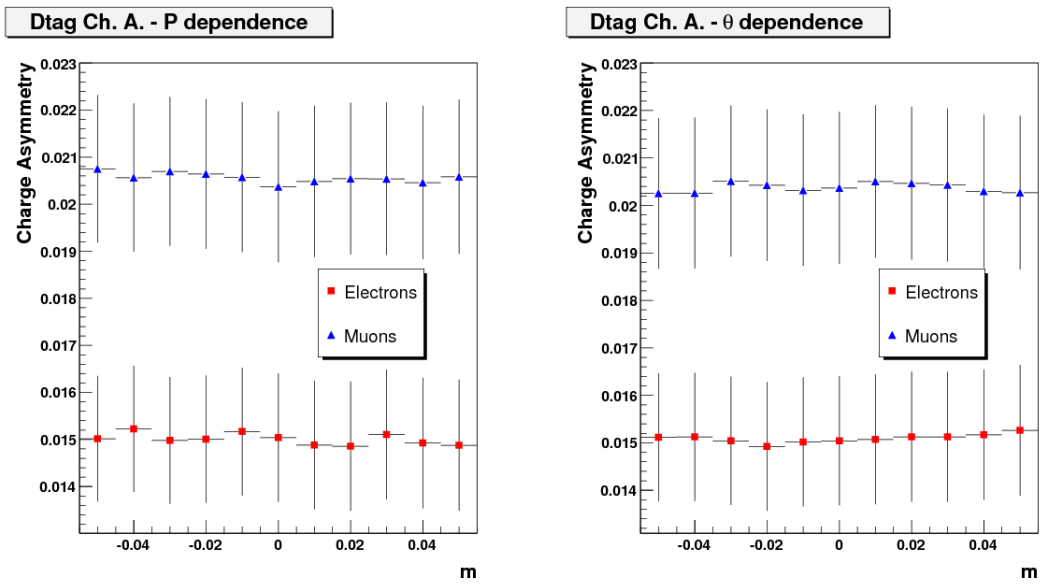

Figure 15: Charge asymmetries for modified $|\vec{p}_L|$ spectra (left plot) and ϑ_L (right) separately for electrons (red squares) and muons (blue triangles).

- *Mixed positive* (MP): (K^+, ℓ^+);
- *Mixed negative* (MN): (K^-, ℓ^-);

Before describing in detail signal and background pdf's, we will summarize in section 5.1 the main detector related contributions affecting our analysis.

5.1 Reconstruction and tagging asymmetries

Theoretical signal and background pdf's have to be properly modified in order to take into account physical and detector related asymmetries. These can be schematically grouped as follows:

1. *Reconstruction Asymmetry.* If ρ is the reconstruction efficiency of a $\ell^+\pi_s^-$ pair and $\bar{\rho}$ is the reconstruction efficiency for its conjugate, we define the reconstruction asymmetry $A_{rec} = (\rho - \bar{\rho})/(\rho + \bar{\rho})$ and the average reconstruction efficiency $R = (\rho + \bar{\rho})/2$. ρ and $\bar{\rho}$ can then be expressed as:

$$\begin{aligned} \rho &= R(1 + A_{rec}) \\ \bar{\rho} &= R(1 - A_{rec}) \end{aligned} \tag{13}$$

   Given that the reconstruction efficiencies for $e^{\pm}\pi_s^{\mp}$ pairs is different from the ones for $\mu^{\pm}\pi_s^{\mp}$, we will distinguish the two lepton flavors in the fit and quote $A_{rec}(e)$ and $A_{rec}(\mu)$.

2. *Tagging Asymmetry (Physics).* We define ω^+ the probability for a B^0 to have among its decay products the hadron h^- and ω^- the probability for a $\overline{B}^0$ to decay to h^+. We have $\Delta\omega = \omega^+ - \omega^-$ and $\omega = (\omega^+ + \omega^-)/2$.

3. *Tagging Asymmetry (Detector).* If τ is the probability that the hadron h^+ is identified as a K^+ and $\bar{\tau}$ the probability that h^- is identified as K^-, we define: $A_{tag} = (\tau - \bar{\tau})/(\tau + \bar{\tau})$ and $T = (\tau + \bar{\tau})/2$. τ and $\bar{\tau}$ can be written as:

$$\begin{aligned} \tau &= T(1 + A_{tag}) \\ \bar{\tau} &= T(1 - A_{tag}) \end{aligned} \tag{14}$$

We will assume that B_{tag} and D_{tag} samples share the same A_{rec} and A_{tag} asymmetries, while ω and $\Delta\omega$ are kept separated because they originate from different underlying physical processes.

Because of these effects, the theoretical pdf's $\mathcal{F}_\chi(s_t, s_m)$, where χ defines the different components (*signal B_{tag}, signal D_{tag}, combinatorial B_{tag}, combinatorial D_{tag}, peaking and continuum*), are related to measured pdf's $\mathcal{F}^{meas}_\chi(s_t, s_m)$, in this way:

$$\begin{aligned} \mathcal{F}^{meas}_\chi(s_t = 1, s_m = -1) &= \rho\tau \left[(1 - \omega^+_\chi)\mathcal{F}_\chi(1,-1) + \omega^-_\chi \mathcal{F}_\chi(-1,1)\right] = \\ &= RT(1 + A_{rec})(1 + A_{tag}) \left[(1 - \omega^+_\chi)\mathcal{F}_\chi(1,-1) + \omega^-_\chi \mathcal{F}_\chi(-1,1)\right] \end{aligned} \tag{15}$$

$$\begin{aligned} \mathcal{F}^{meas}_\chi(s_t = 1, s_m = 1) &= \bar{\rho}\tau \left[(1 - \omega^+_\chi)\mathcal{F}_\chi(1,1) + \omega^-_\chi \mathcal{F}_\chi(-1,-1)\right] = \\ &= RT(1 - A_{rec})(1 + A_{tag}) \left[(1 - \omega^+_\chi)\mathcal{F}_\chi(1,1) + \omega^-_\chi \mathcal{F}_\chi(-1,-1)\right] \end{aligned} \tag{16}$$

$$\begin{aligned} \mathcal{F}^{meas}_\chi(s_t = -1, s_m = -1) &= \bar{\rho}\bar{\tau} \left[(1 - \omega^-_\chi)\mathcal{F}_\chi(-1,-1) + \omega^+_\chi \mathcal{F}_\chi(1,1)\right] = \\ &= RT(1 - A_{rec})(1 - A_{tag}) \left[(1 - \omega^-_\chi)\mathcal{F}_\chi(-1,-1) + \omega^+_\chi \mathcal{F}_\chi(1,1)\right] \end{aligned} \tag{17}$$

$$\begin{aligned} \mathcal{F}^{meas}_\chi(s_t = -1, s_m = 1) &= \rho\bar{\tau} \left[(1 - \omega^-_\chi)\mathcal{F}_\chi(-1,1) + \omega^+_\chi \mathcal{F}_\chi(1,-1)\right] = \\ &= RT(1 + A_{rec})(1 - A_{tag}) \left[(1 - \omega^-_\chi)\mathcal{F}_\chi(-1,1) + \omega^+_\chi \mathcal{F}_\chi(1,-1)\right] \end{aligned} \tag{18}$$

where s_t and s_m have been defined in section 2.

The resolution functions convoluted with the $\mathcal{F}^{meas}_\chi(s_t, s_m)$ defined above will be discussed in the following sections 5.2- 5.9 for each component of the global pdf.

5.2 Signal B_{tag}

The theoretical pdf's $\mathcal{F}_{B_{tag},sig}(s_t, s_m)$ for signal B_{tag} events are those described in section 2.

The resolution model we need to use is complicated by the fact that a large fraction of B_{tag} kaons originate from *cascade* decays ($b \to c \to K$); the effect of the finite lifetime of the charmed meson and the experimental boost cause a distortion towards negative values of the Δt distribution. This effect is accounted for by using gaussians convoluted with a decaying exponential (Gexp's) instead of simple gaussians in the resolution model.

Moreover, the dependence on $|\vec{p}_K|$ of the resolution function has to be parameterized. The resolution model, for *signal B_{tag}* events, is defined as follows:

$$R_{B_{tag},sig}(\delta\Delta t, \sigma\Delta t, |\vec{p}_K|) = f_n \; exp\left(-\frac{(\delta\Delta t - o_n)^2}{2(s_n(|\vec{p}_K|)\,\sigma\Delta t)^2}\right) +$$

$$
\begin{aligned}
&+ \quad |1 - f_n - f_o| \; exp\left(-\frac{(\delta\Delta t - o_w)^2}{2(s_w(|\vec{p}_K|)\,\sigma\Delta t)^2}\right) + \\
&+ \quad f_o \; exp\left(-\frac{(\delta\Delta t - o_o)^2}{2s_o^2}\right) \qquad (19)
\end{aligned}
$$

where $\delta\Delta t = \Delta t_{true} - \Delta t_{meas}$ and s_x and o_x $(x = n, w, o)$ are the offsets and widths, respectively, of the gaussian components.

$R_{B_{tag},sig}(\delta\Delta t, \sigma\Delta t, |\vec{p}_K|)$ is convoluted with two decaying exponentials:

$$
\begin{aligned}
\mathcal{R}_{B_{tag},sig}(\delta\Delta t, \sigma\Delta t, |\vec{p}_K|) &= (1 - f_{G2}(|\vec{p}_K|))\; R_{B_{tag},sig}(\delta\Delta t, \sigma\Delta t, |\vec{p}_K|) \otimes exp\left(-\frac{\delta\Delta t}{\tau_{G1}}\right) + \\
&+ \quad f_{G2}(|\vec{p}_K|)\; R_{B_{tag},sig}(\delta\Delta t, \sigma\Delta t, |\vec{p}_K|) \otimes exp\left(-\frac{\delta\Delta t}{\tau_{G2}(|\vec{p}_K|)}\right) \qquad (20)
\end{aligned}
$$

The dependence on $|\vec{p}_K|$ of some of the parameters entering the resolution model is

$$
\begin{aligned}
s_x(|\vec{p}_K|) &= s_{x,0} + \frac{s_{x,1}}{\sqrt{|\vec{p}_K|}} \qquad x = n, w \qquad (21)\\
\tau_{G2}(|\vec{p}_K|) &= \tau_{G2,0} + \frac{\tau_{G2,1}}{\sqrt{|\vec{p}_K|}} \qquad (22)\\
f_{G2}(|\vec{p}_K|) &= f_{G2,0} + f_{G2,1}|\vec{p}_K| \qquad (23)
\end{aligned}
$$

The left plot of figure 16 shows the resulting resolution model for a kaon with $|\vec{p}_K| = 1$ GeV/c.

The mistag probability ω^+ (ω^-) of incorreclty tagging a B^0 ($\overline{B}^0$) reduces the statistical significance of our measurement by the dilution factor $D = (1 - 2\omega)$. The dilution is also dependent linearly on $|\vec{p}_K|$:

$$
D(|\vec{p}_K|) = D_0 + D_1\,|\vec{p}_K| \qquad (24)
$$

5.3 Signal D_{tag}

Signal D_{tag} events are parameterized by using a double exponential with an effective D^0 lifetime τ_{D^0}. This pdf is convoluted with the following resolution model:

$$
\begin{aligned}
R_{D_{tag},sig}(\delta\Delta t, \sigma\Delta t, |\vec{p}_K|) &= f_{nn}\; exp\left(-\frac{(\delta\Delta t - o_{nn})^2}{2(s_{nn}\,\sigma\Delta t)^2}\right) + \\
&+ \quad f_n \; exp\left(-\frac{(\delta\Delta t - o_n)^2}{2(s_n(|\vec{p}_K|)\,\sigma\Delta t)^2}\right) + \\
&+ \quad |1 - f_{nn} - f_n - f_o| \; exp\left(-\frac{(\delta\Delta t - o_w)^2}{2(s_w(|\vec{p}_K|)\,\sigma\Delta t)^2}\right) + \\
&+ \quad f_o \; exp\left(-\frac{(\delta\Delta t - o_o)^2}{2s_o^2}\right) \qquad (25)
\end{aligned}
$$

The resolution function $\mathcal{R}D_{tag}, sig(\delta\Delta t, \sigma\Delta t, |\vec{p}_K|)$ is computed by convoluting each of the gaussian components with a Gexp with lifetimes τ_{nn}, τ_n, τ_w and $\tau_o(|\vec{p}_K|)$.

As in the B_{tag} case, we allow a dependence on $|\vec{p}_K|$ for the widths of the narrow and the wide components; moreover we allow the lifetime of the outlier Gexp to have a dependence on the kaon momentum:

$$s_x(|\vec{p}_K|) = s_{x,0} + \frac{s_{x,1}}{\sqrt{|\vec{p}_K|}} \quad x = n, w \tag{26}$$

$$\tau_o(|\vec{p}_K|) = \tau_{o,0} + \frac{\tau_{o,1}}{|\vec{p}_K|}. \tag{27}$$

The right plot of figure 16 shows the resulting resolution model for a kaon with $|\vec{p}_K| = 1$ GeV/c.

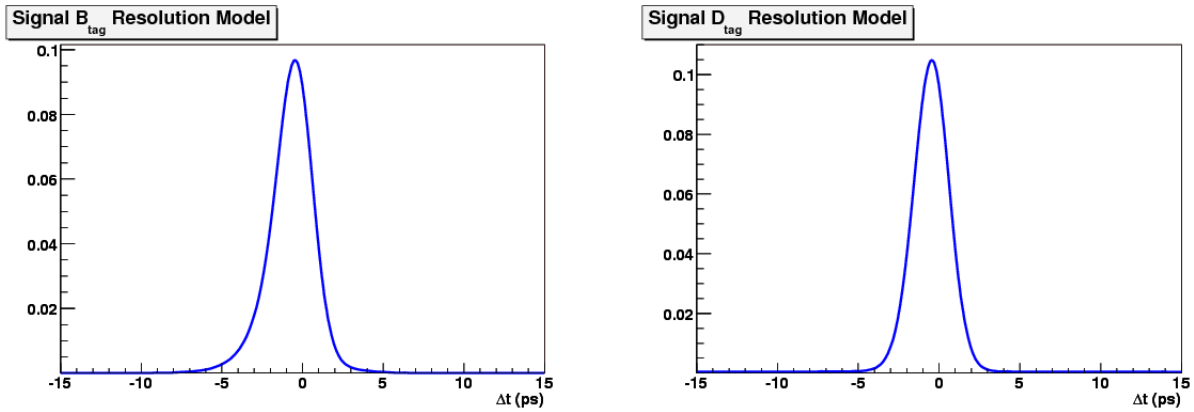

Figure 16: Resolution models for B_{tag} (left plot) and D_{tag} (right) signal events. The models shown are referred to a kaon with $|\vec{p}_K| = 1$ GeV/c.

5.4 Combinatorial B_{tag} ($B^0\overline{B}^0$)

For this category of events, the same pdf and resolution model described in section 5.2 is used. Given that in this case the ℓ,π_{soft} are uncorrelated the parameters τ_{B^0} and Δm_d have no direct physical interpretation but are used as two effective parameters.

5.5 Combinatorial B_{tag} (B^+B^-)

The pdf is a double exponential, decaying with an effective lifetime $\tau_{Bch,bkg}$.

The resolution model is defined as follows:

$$\begin{aligned} R_{Bch,bkg}(\delta\Delta t, \sigma\Delta t, |\vec{p}_K|) &= f_n\, exp\left(-\frac{(\delta\Delta t - o_n)^2}{2(s_n(|\vec{p}_K|)\,\sigma\Delta t)^2}\right) + \\ &+ |1 - f_n - f_o|\, exp\left(-\frac{(\delta\Delta t - o_w)^2}{2(s_w(|\vec{p}_K|)\,\sigma\Delta t)^2}\right) + \\ &+ f_o\, exp\left(-\frac{(\delta\Delta t - o_o)^2}{2s_o^2}\right) \end{aligned} \tag{28}$$

$R_{Bch,bkg}(\delta\Delta t, \sigma\Delta t, |\vec{p}_K|)$ is convoluted with an exponential:

$$\mathcal{R}_{Bch,bkg}(\delta\Delta t, \sigma\Delta t, |\vec{p}_K|) = R_{Bch,bkg}(\delta\Delta t, \sigma\Delta t, |\vec{p}_K|) \otimes exp\left(-\frac{\delta\Delta t}{\tau_G}\right)$$

The only parameters depending on $|\vec{p}_K|$ are:

$$s_x(|\vec{p}_K|) = s_{x,0} + \frac{s_{x,1}}{\sqrt{|\vec{p}_K|}} \quad x = n, w$$

5.6 Combinatorial D_{tag}

We use the same pdf found for signal D_{tag} events for both $B^0\overline{B}^0$ and B^+B^- combinatorial events. While for B^+B^- the parameters are the same we use, for signal D_{tag} we use independent parameters of $B^0\overline{B}^0$ combinatorial events.

5.7 Peaking B_{tag}

The same pdf and resolution model used in 5.5 is also used for peaking background B_{tag} events, with the same dependence on $|\vec{p}_K|$ for s_n and s_o.

5.8 Peaking D_{tag}

The same resolution model used for signal D_{tag} is used (see section 5.3), forcing all the parameters to be the same for the two samples.

5.9 Continuum background

The pdf used for modeling the background originating from continuum events is a decaying exponential with effective lifetime τ_{off}.

The resolution model is very similar to the one used for signal B_{tag}:

$$\begin{aligned} R_{off}(\delta\Delta t, \sigma\Delta t, |\vec{p}_K|) &= f_n\, exp\left(-\frac{(\delta\Delta t - o_n)^2}{2(s_n(|\vec{p}_K|)\,\sigma\Delta t)^2}\right) + \\ &+ |1 - f_n - f_o|\, exp\left(-\frac{(\delta\Delta t - o_w)^2}{2(s_w(|\vec{p}_K|)\,\sigma\Delta t)^2}\right) + \\ &+ f_o\, exp\left(-\frac{(\delta\Delta t - o_o)^2}{2s_o^2}\right) \end{aligned} \tag{29}$$

$R_{off}(\delta\Delta t, \sigma\Delta t, |\vec{p}_K|)$ is convoluted with two exponentials:

$$\begin{aligned} \mathcal{R}_{off}(\delta\Delta t, \sigma\Delta t, |\vec{p}_K|) &= (1 - f_{G2})\, R_{off}(\delta\Delta t, \sigma\Delta t, |\vec{p}_K|) \otimes exp\left(-\frac{\delta\Delta t}{\tau_{G1}}\right) + \\ &+ f_{G2}\, R_{off}(\delta\Delta t, \sigma\Delta t, |\vec{p}_K|) \otimes exp\left(-\frac{\delta\Delta t}{\tau_{G2}}\right) \end{aligned} \tag{30}$$

The basical difference with respect to the resolution model used in signal B_{tag} events is that the only parameters depending on $|\vec{p}_K|$ are the widths of the narrow and wide gaussians:

$$s_x(|\vec{p}_K|) = s_{x,0} + \frac{s_{x,1}}{\sqrt{|\vec{p}_K|}} \quad x = n, w$$

5.10 CP-eigenstates

A small subsample (of the order of 3 %) of our selected events originate from B^0 decays to CP-eigenstates (mostly $B^0 \to D^* \bar{D}^*$). Given that the probability of having a K^+ is equal to the one of having a K^- and that there is interference between mixing and decay, these events need to be treated separately from the rest of B_{tag} B^0 decays.

We model these decays with the usual pdf:

$$\mathcal{F}_{CP-eigen} = \frac{\Gamma}{4} e^{-\Gamma|\Delta t|} \left[1 \pm S_{eff} \sin(\Delta m_d \Delta t) \pm C_{eff} \cos(\Delta m_d \Delta t)\right] \tag{31}$$

where the + sign applies to B_{rec} tagged as a B^0 and - to B_{rec} tagged as a $\overline{B}^0$.

We take the same resolution model we use for the other B^0 B_{tag} events.

Given the smallness of this sample, we fit the C_{eff} and S_{eff} parameters to the Monte Carlo and fix their values on the nominal fit to the data.

6 Validation on generic Monte Carlo

In this section, we describe the different steps of the validation of our fit model on Monte Carlo. Besides the last sub-section, the samples used in this section correspond to generic Run1-4 Monte Carlo.

Throughout this section, every fit is performed keeping $|q/p| - 1$, $\Delta\Gamma$, b and c fixed to 0, that is to the value used in the generation of generic MC.

We also report the values of tagging and reconstruction asymmetries; for the latter, we separate the cases when the B_{rec} lepton is an electron from the muon case.

The purpose of some of the fits which are shown here, is just to debug our machinery, therefore we report the results even if a fit has not properly converged and the errors associated to the parameters are not realistic.

6.1 Signal B_{tag} - true Δt, true tag

As a first step of the validation process, we fit signal B_{tag} events using the Monte Carlo truth for both Δt and the flavor of B_{tag}.

Table 6: Results of the fit to generic Run1-4 MC, using true Δt and the true flavor of B_{tag}.

Parameter	Generated value	Fit result
τ_{B^0}	1.540	1.5385 ± 0.0008
Δm_d	0.489	0.4834 ± 0.0002
A_{tag}	-	0.0084 (fixed)
$A_{rec}(e)$	-	0.0070 (fixed)
$A_{rec}(\mu)$	-	0.0129 (fixed)

We let τ_{B^0} and Δm_d as the only free parameters in the fit. Results are in good agreement with expectations and are reported in table 6 and in figure 17.

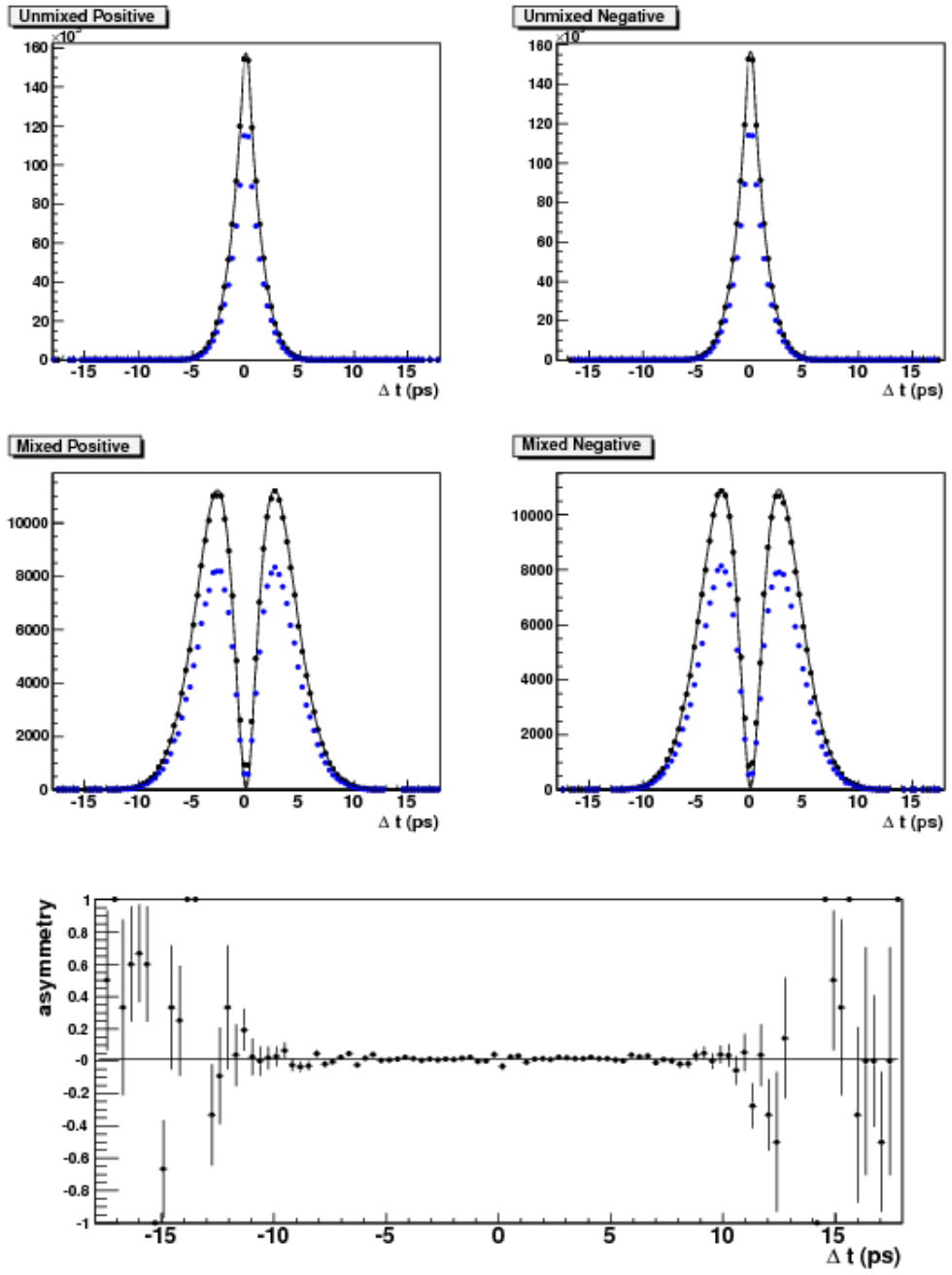

Figure 17: Fitted distributions for the four samples (top plots). The generated Δt value has been used and B_{tag} has been tagged using the MC truth. Black dots correspond to the whole B_{tag} sample, while blue ones show the *cascades* component. The asymmetry is shown in the bottom plot.

6.2 Signal B_{tag} - true Δt, experimental tag

Table 7 and figure 18 summarize the results of the fit on signal B_{tag} sample, using the MC truth for Δt, but considering the experimental dilution.

Besides τ_{B^0} and Δm_d only the parameters D_0, D_1 and $\Delta\omega$ are left floating in the fit. Again, the fit results are consistent with expectations.

Table 7: Results of the fit to generic Run1-4 MC, using true Δt and the flavor of $B_{tag}$is determined considering the experimental dilution.

Parameter	Fit result
τ_{B^0}	1.5380 ± 0.0009
Δm_d	0.4788 ± 0.0006
A_{tag}	0.0088 (fixed)
$A_{rec}(e)$	0.0050 (fixed)
$A_{rec}(\mu)$	0.0092 (fixed)
D_0	0.3590 ± 0.0019
D_1	0.2372 ± 0.0024
$\Delta\omega$	-0.0083 ± 0.0005

6.3 Signal B_{tag} - measured Δt, true tag

We repeat the fit by using the Monte Carlo truth information for the flavor of B_{tag} and the measured value of Δt, leaving the parameters of the resolution floating. Results are reported in table 8 and figure 19

Due to some problems in the final stages of the fit, the errors associated to the output parameters are unrealistically small, but the shapes are correctly reproduced by the global pdf.

6.4 Signal B_{tag} - measured Δt, experimental tag

We now fit the B_{tag} sample using the reconstructed Δt and the realistic tagging. All the parameters separately left free in the two previous stages of the validation are floating.

The results are reported in table 9 and figure 20.

6.5 Signal D_{tag} - measured Δt, experimental tag

We apply the pdf and the resolution model described in section 5.3 to fit only signal D_{tag} events. The generic Run1-4 Monte Carlo has been used; results are shown in table 10 and figure 21.

6.6 $B\overline{B}$ combinatorial - measured Δt, experimental tag

In this section we show (without numerical outputs) the results of the fits of each background components, using the pdf's and the resolution models described in section 5.

Figures 22-25 show the fitted distributions for the various $B\overline{B}$ combinatorial samples.

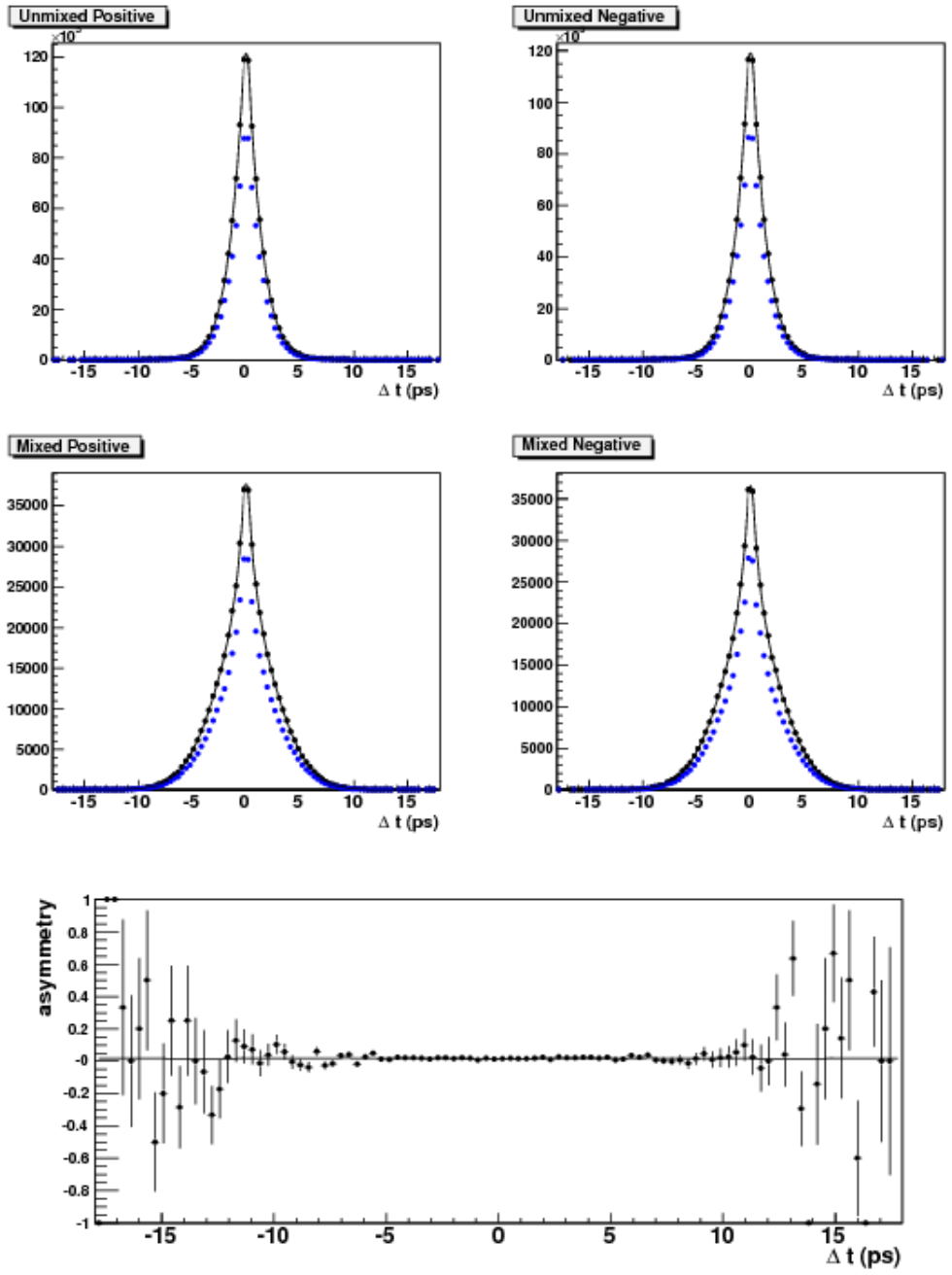

Figure 18: Fitted distributions for the four samples (top plots). The generated Δt value has been used, while the flavor of B_{tag} is determined with the experimental dilution. Black dots correspond to the whole B_{tag} sample, while blue ones show the *cascades* component. The asymmetry is shown in the bottom plot.

Table 8: Results of the fit to generic Run1-4 MC, using true Δt and the true of $B_{tag}$is determined considering the experimental dilution.

Parameter	Fit result
τ_{B^0}	1.5269 ± 0.0001
Δm_d	0.4849 ± 0.0001
A_{tag}	0.0088 (fixed)
$A_{rec}(e)$	0.0050 (fixed)
$A_{rec}(\mu)$	0.0092 (fixed)
f_n	0.8990 ± 0.0001
f_o	0.0451 ± 0.0001
o_n	0.0062 ± 0.0001
o_w	-0.1033 ± 0.0001
o_o	0.0000 (fixed)
$s_{n,0}$	0.5653 ± 0.0001
$s_{n,1}$	0.4063 ± 0.0001
$s_{w,0}$	1.2140 ± 0.0001
$s_{w,1}$	1.0339 ± 0.0001
s_o	28.172 ± 0.0001
f_{G2}	0.3580 ± 0.0001
τ_{G1}	0.1152 ± 0.0001
$\tau_{G2,0}$	1.1102 ± 0.0001
$\tau_{G2,1}$	-0.1463 ± 0.0001

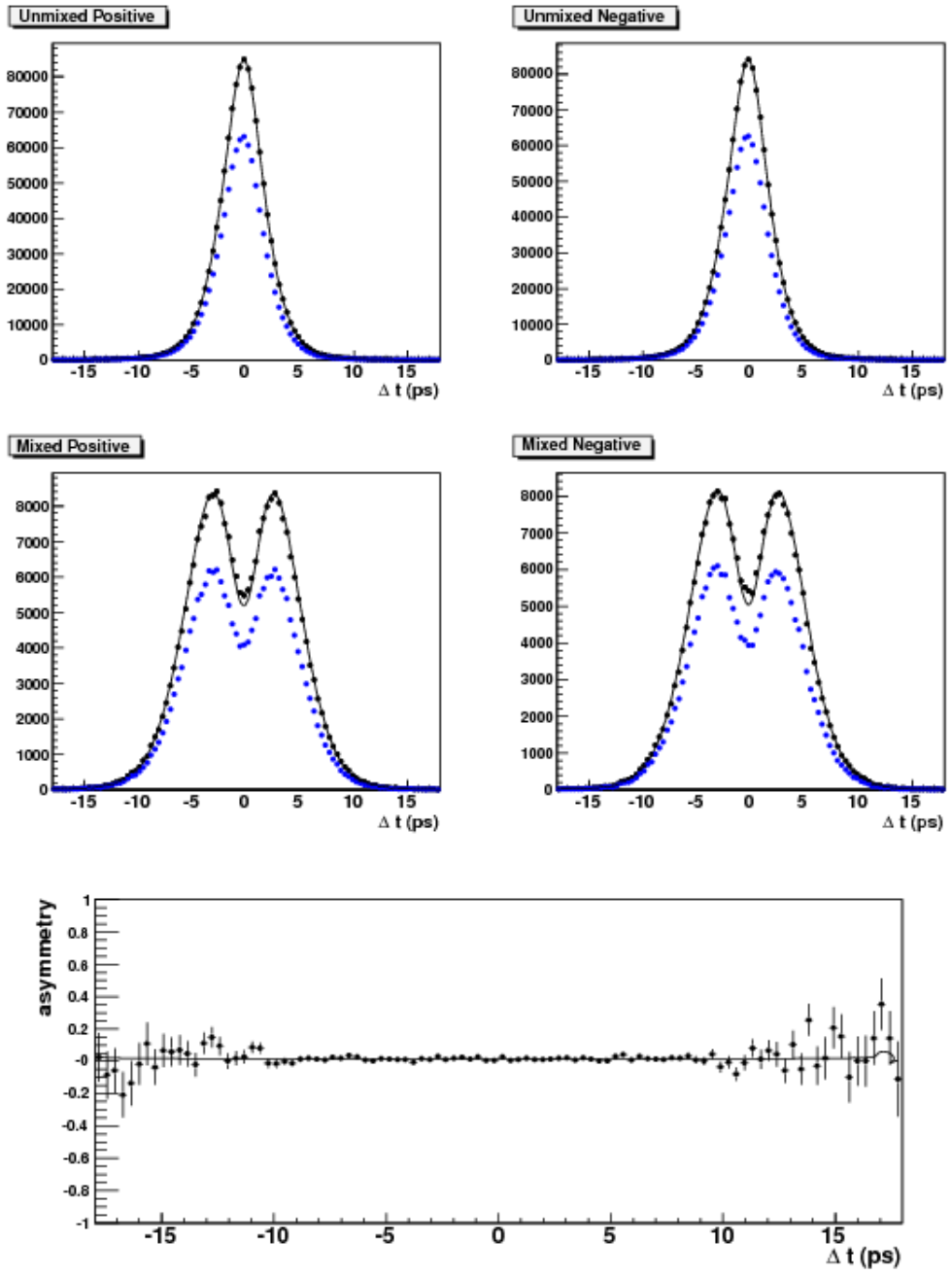

Figure 19: Fitted distributions for the four samples (top plots). The measured Δt value has been used, while the flavor of B_{tag} is got from MC truth. Black dots correspond to the whole B_{tag} sample, while blue ones show the *cascades* component. The asymmetry is shown in the bottom plot.

Table 9: Results of the fit to generic Run1-4 MC, using measured Δt and realistic tagging.

Parameter	Fit result
τ_{B^0}	1.5322 ± 0.0002
Δm_d	0.4838 ± 0.0003
A_{tag}	0.0088 ± 0.0003
$A_{rec}(e)$	0.0050 ± 0.0003
$A_{rec}(\mu)$	0.0092 ± 0.0003
D_0	0.3915 ± 0.0005
D_1	0.1735 ± 0.0003
$\Delta\omega$	-0.0087 ± 0.0003
f_n	0.9018 ± 0.0001
f_o	0.0318 ± 0.0001
o_n	0.0181 ± 0.0009
o_w	-0.1442 ± 0.0008
o_o	0.0000 (fixed)
$s_{n,0}$	0.5656 ± 0.0022
$s_{n,1}$	0.3997 ± 0.0019
$s_{w,0}$	1.2346 ± 0.0012
$s_{w,1}$	1.0370 ± 0.0010
s_o	28.415 ± 0.0251
f_{G2}	0.3684 ± 0.0015
τ_{G1}	0.1183 ± 0.0035
$\tau_{G2,0}$	1.1115 ± 0.0048
$\tau_{G2,1}$	-0.1892 ± 0.0044

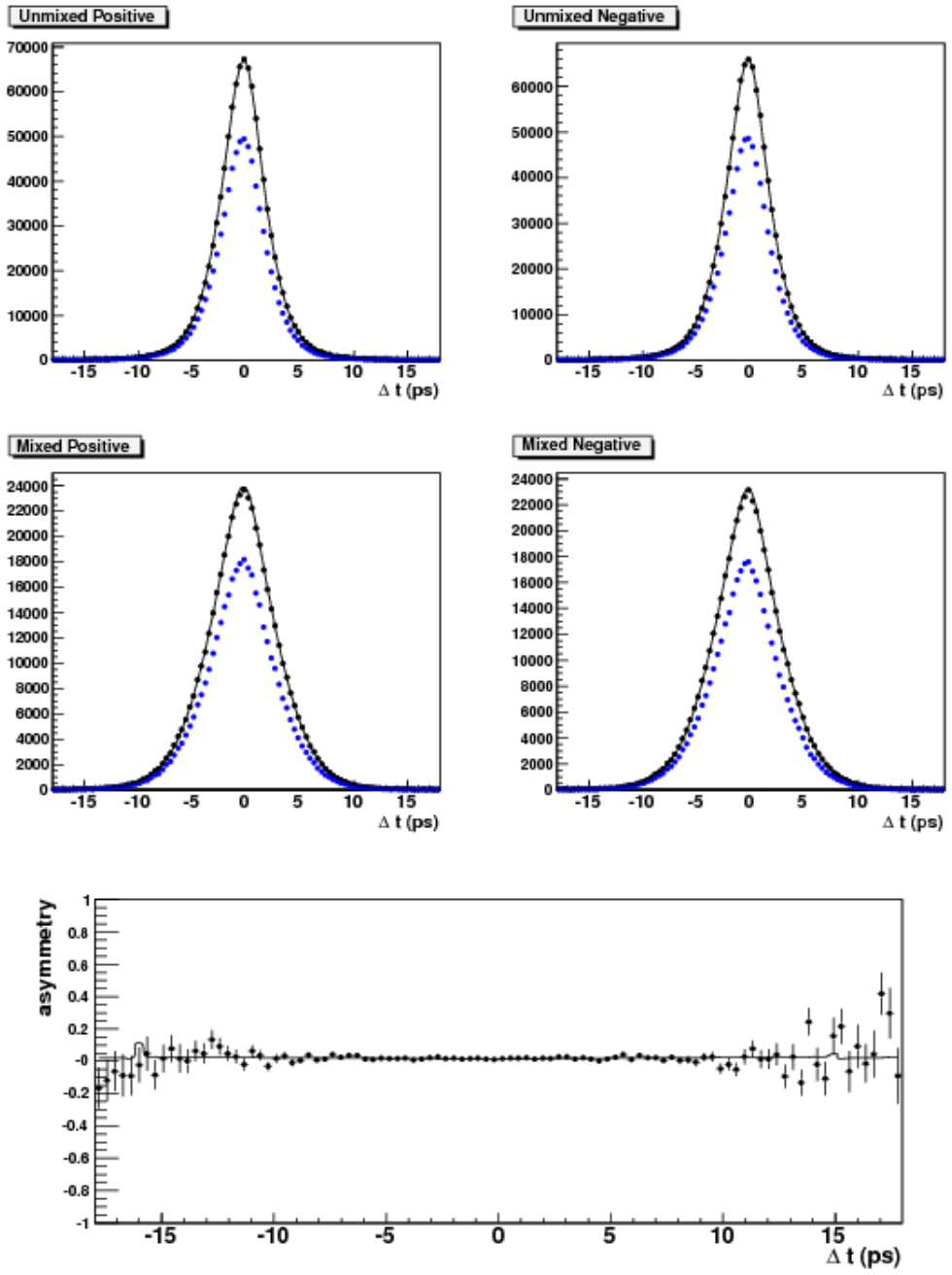

Figure 20: Fitted distributions for the four samples (top plots). The measured Δt value has been used and the flavor of B_{tag} is determined with the experimental dilution. Black dots correspond to the whole B_{tag} sample, while blue ones show the *cascades* component. The asymmetry is shown in the bottom plot.

Table 10: Results of the fit to signal D_{tag} on generic Run1-4 MC, using measured Δt and realistic tagging.

Parameter	Fit result
A_{tag}	0.0071 ± 0.0006
$A_{rec}(e)$	0.0062 ± 0.0008
$A_{rec}(\mu)$	0.0122 ± 0.0010
D_0	0.4083 (fixed)
D_1	0.1961 (fixed)
$\Delta\omega$	-0.0092 (fixed)
f_{nn}	0.0980 ± 0.0002
f_n	0.9237 ± 0.0003
f_o	0.0351 ± 0.0003
o_{nn}	0.0714 ± 0.0048
o_n	-0.1051 ± 0.0013
o_w	-0.3251 ± 0.0136
o_o	1.4675 ± 1.1398
s_{nn}	0.7028 ± 0.0017
$s_{n,0}$	0.6044 ± 0.0009
$s_{n,1}$	0.4330 ± 0.0006
$s_{w,0}$	1.0922 ± 0.0113
$s_{w,1}$	1.2415 ± 0.0097
s_o	24.212 ± 0.0034
τ_{nn}	0.0441 ± 0.0006
τ_n	0.3992 ± 0.0012
τ_w	0.8403 ± 0.0103
$\tau_{o,0}$	1.6898 ± 0.0002
$\tau_{o,1}$	0.0029 ± 0.0002

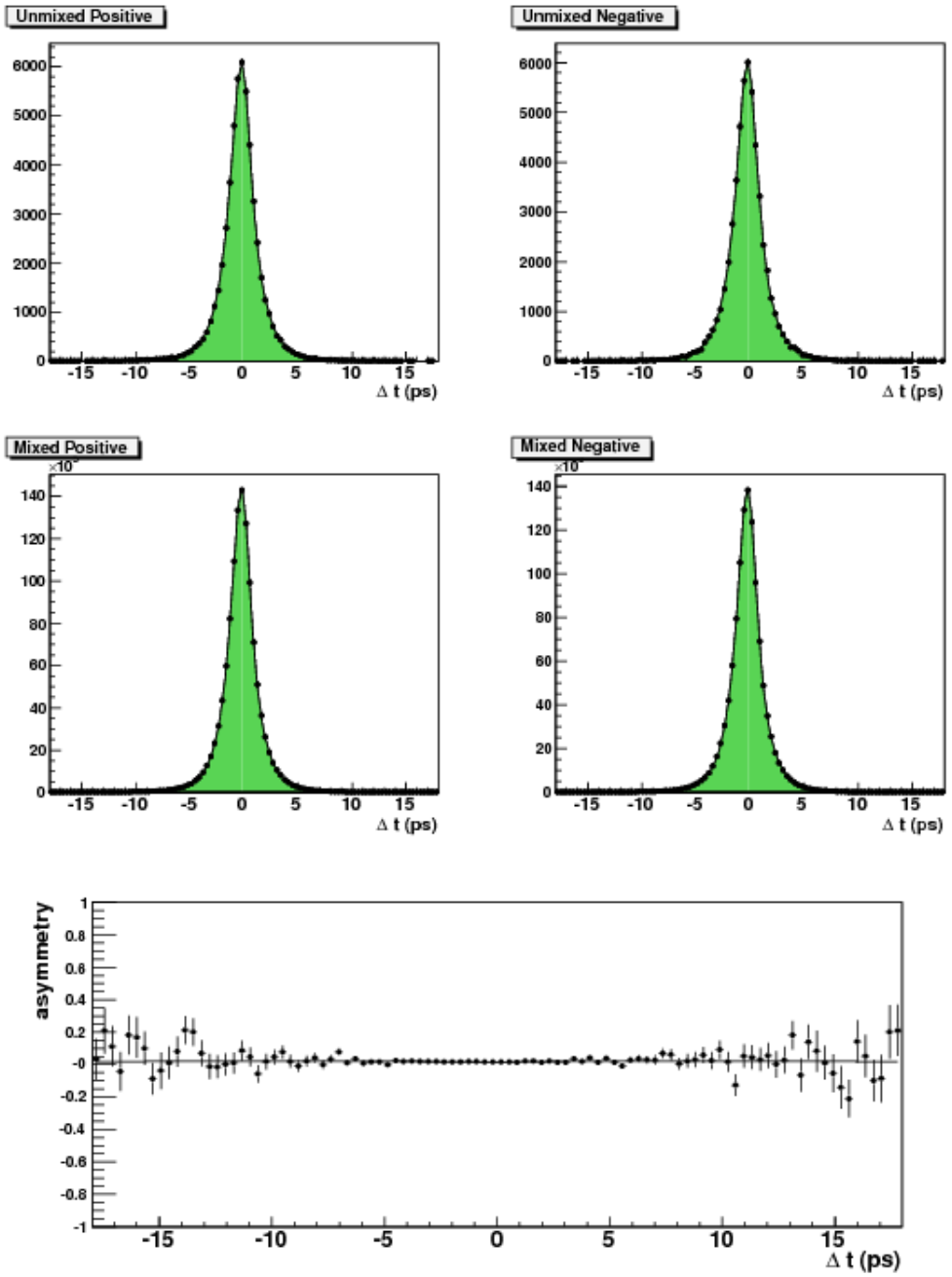

Figure 21: Fitted distributions for the four samples (top plots) of signal D_{tag} events. The asymmetry is shown in the bottom plot.

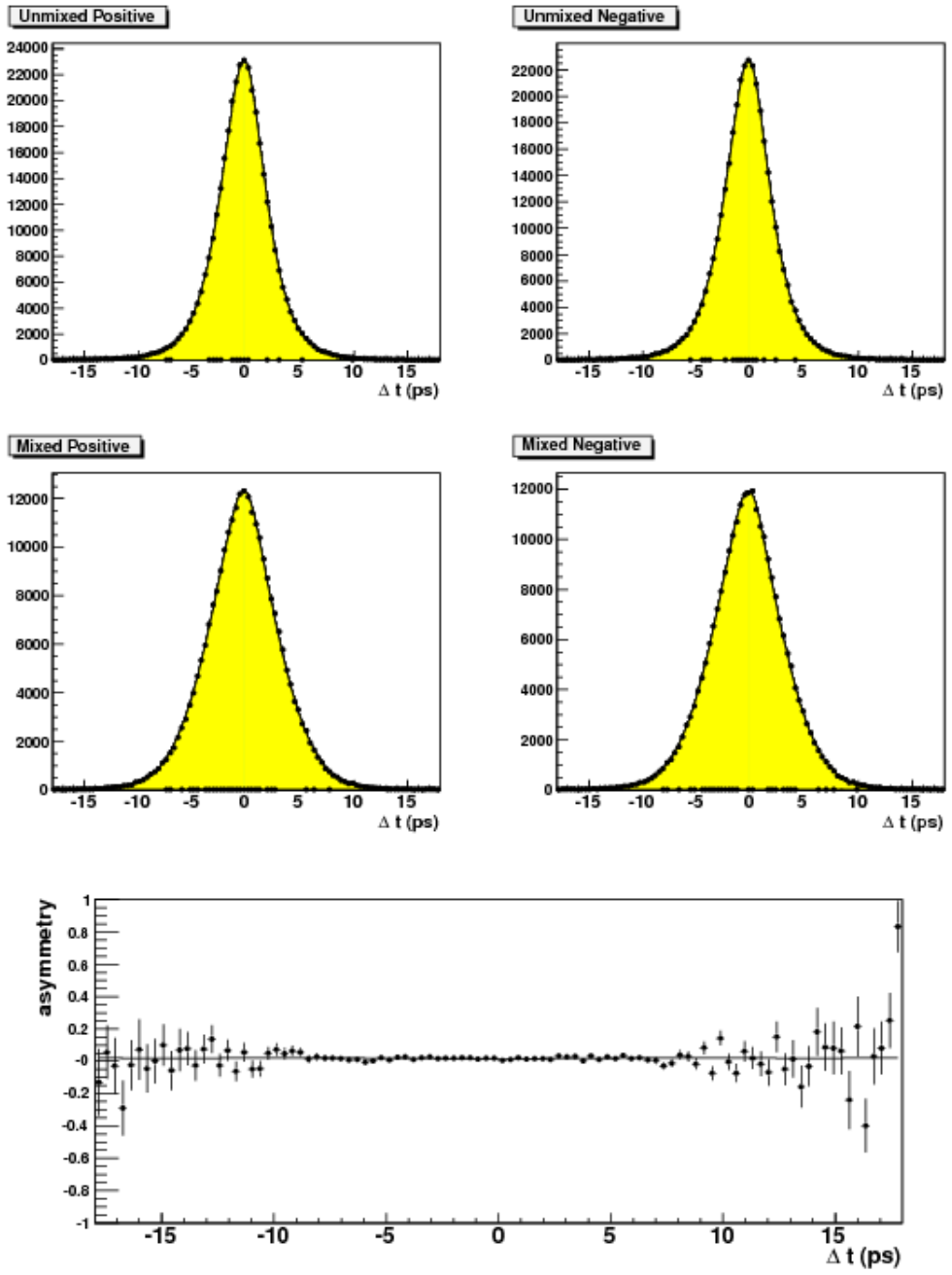

Figure 22: Fitted distributions for $B^0\overline{B}^0$ combinatorial B_{tag} events.

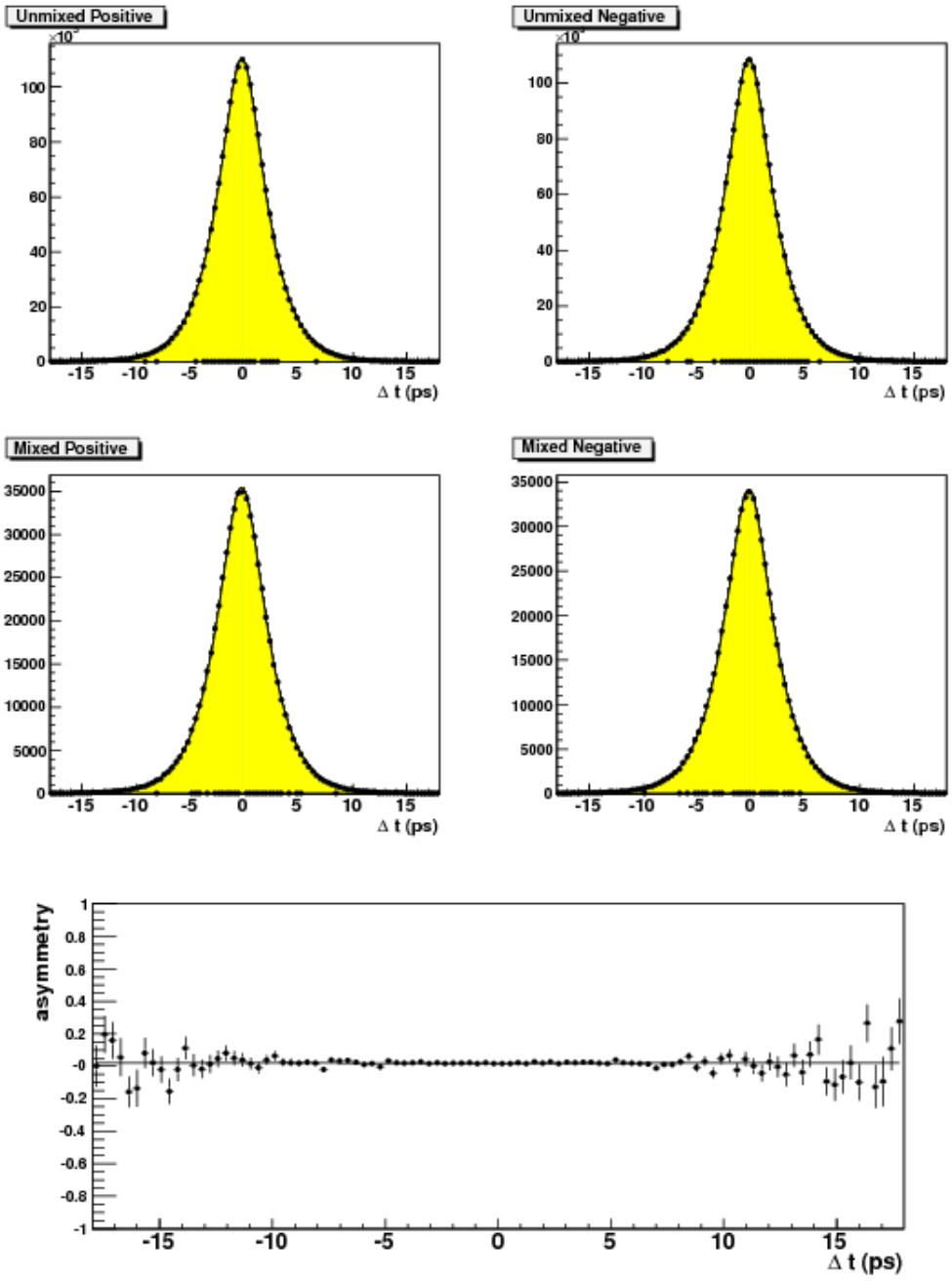

Figure 23: Fitted distributions for B^+B^- combinatorial B_{tag} events.

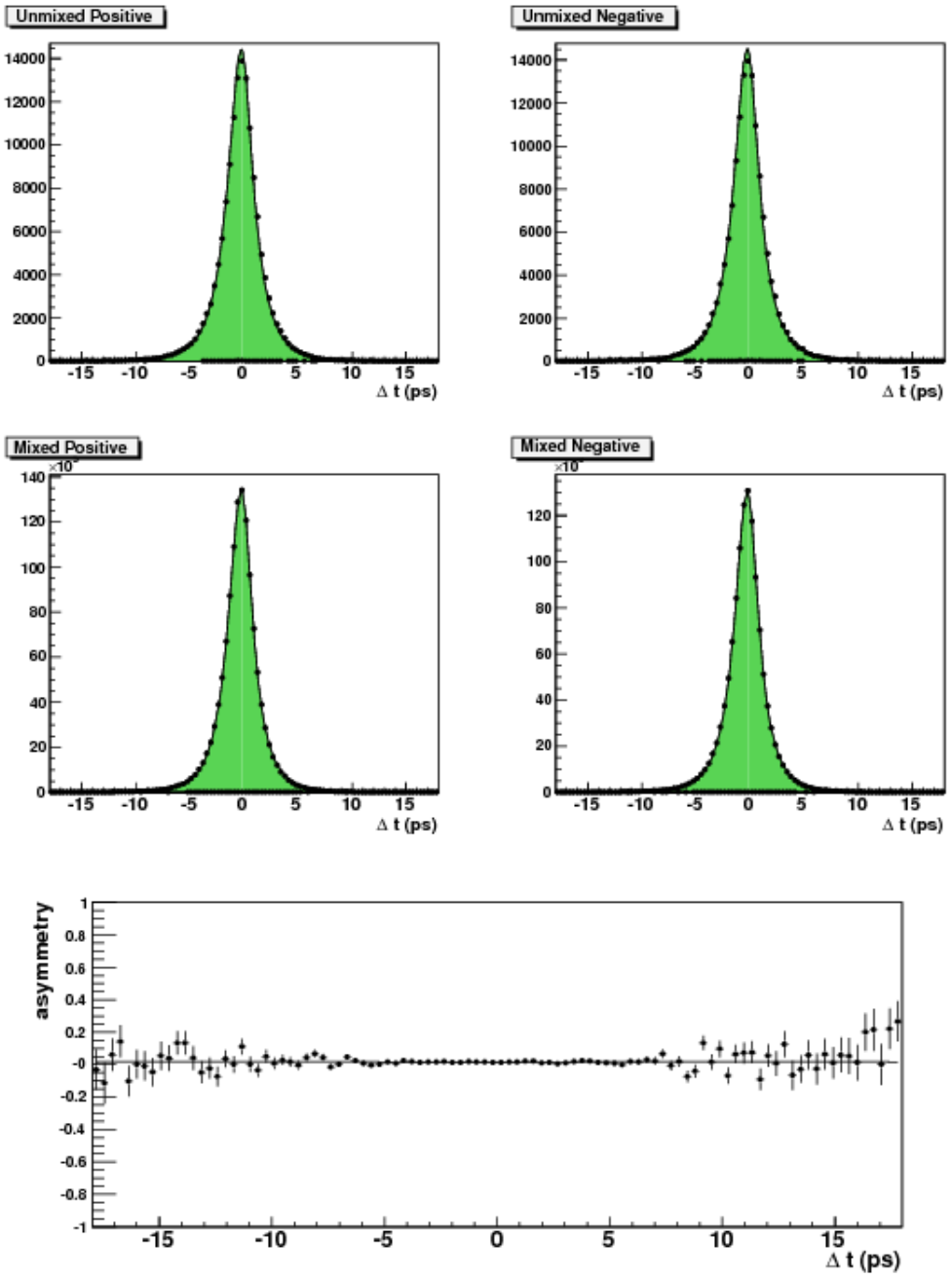

Figure 24: Fitted distributions for $B^0\overline{B}^0$ combinatorial D_{tag} events.

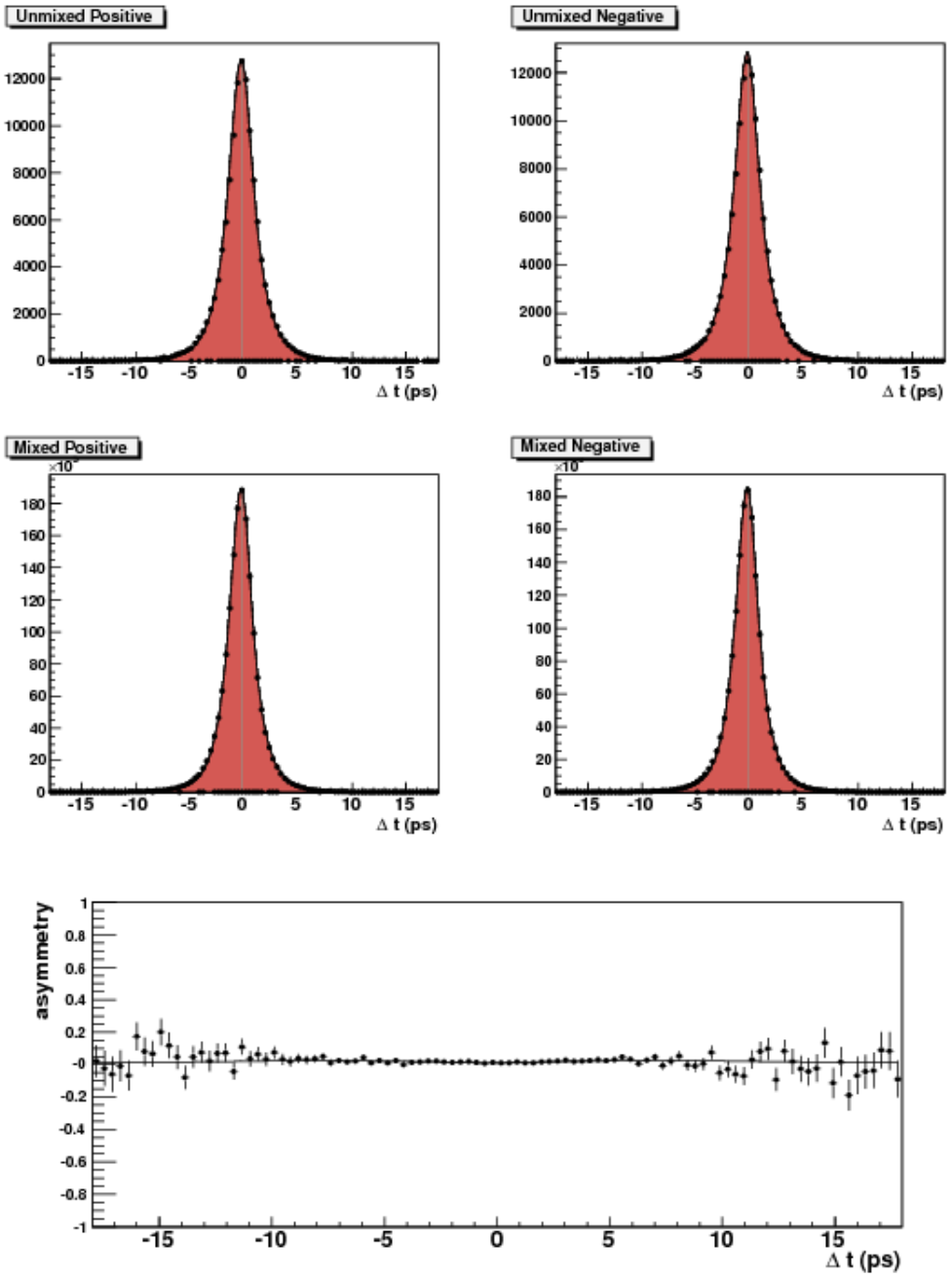

Figure 25: Fitted distributions for B^+B^- combinatorial D_{tag} events.

6.7 Peaking B^+B^- - measured Δt, experimental tag

Figure 26 shows the fitted distributions of peaking B^+B^- B_{tag} events.

We fit the distributions of D_{tag} events coming from $B^{\pm}$ decays using the same model which describes the signal D_{tag} sample.

Figure 27 shows the Δt distributions of peaking D_{tag} events with overlayed the fitting function obtained for the signal D_{tag} sample. It can be seen that the agreement is pretty good and justifies the choice of using the same model for the two parameters.

6.8 Continuum background

We use the off-peak data sample to study the contribution of *continuum* events.

Table 11 and figure 28 show the results of a fit to off-peak Run1-4 events, using the pdf and the resolution model described in 5.9.

Table 11: Results of the fit to off-peak events.

Parameter	Fit result
τ_{off}	0.4431 ± 0.0055
f_n	0.8097 ± 0.0087
f_o	0.0200 ± 0.0006
o_n	-0.0249 ± 0.0050
o_w	-0.1442 ± 0.0283
o_o	0. (fixed)
$s_{n,0}$	0.5840 ± 0.0200
$s_{n,1}$	0.3610 ± 0.0167
$s_{w,0}$	2.1348 ± 0.0263
$s_{w,1}$	0.0000 ± 0.0006
s_o	6.1610 ± 0.0001
f_{G2}	0.2997 ± 0.3856
τ_{G1}	0.0000 ± 0.0025
τ_{G2}	0.1000 ± 1.1033

6.9 CP-eigenstates

We select from our generic Run1-5 $B^0\overline{B}^0$ Monte Carlo sample every decay of a B^0 meson on the tag side to any CP-eigenstate.

We fit this sample, as usual separately for the four different combination of lepton and kaon charges, using the pdf of section 5.10. We keep the same parameters of the resolutions found for generic B_{tag} events, and leave free only the two effective parameter governing the CP behavior.

Numerical results can be found in table 12, while the plots are shown in figure 29.

We fix in the nominal fit C_{eff} and S_{eff} to the values we find in this section. Systematic uncertainties will be estimated by varying those parameters inside an interval which covers our uncertainty in their determination.

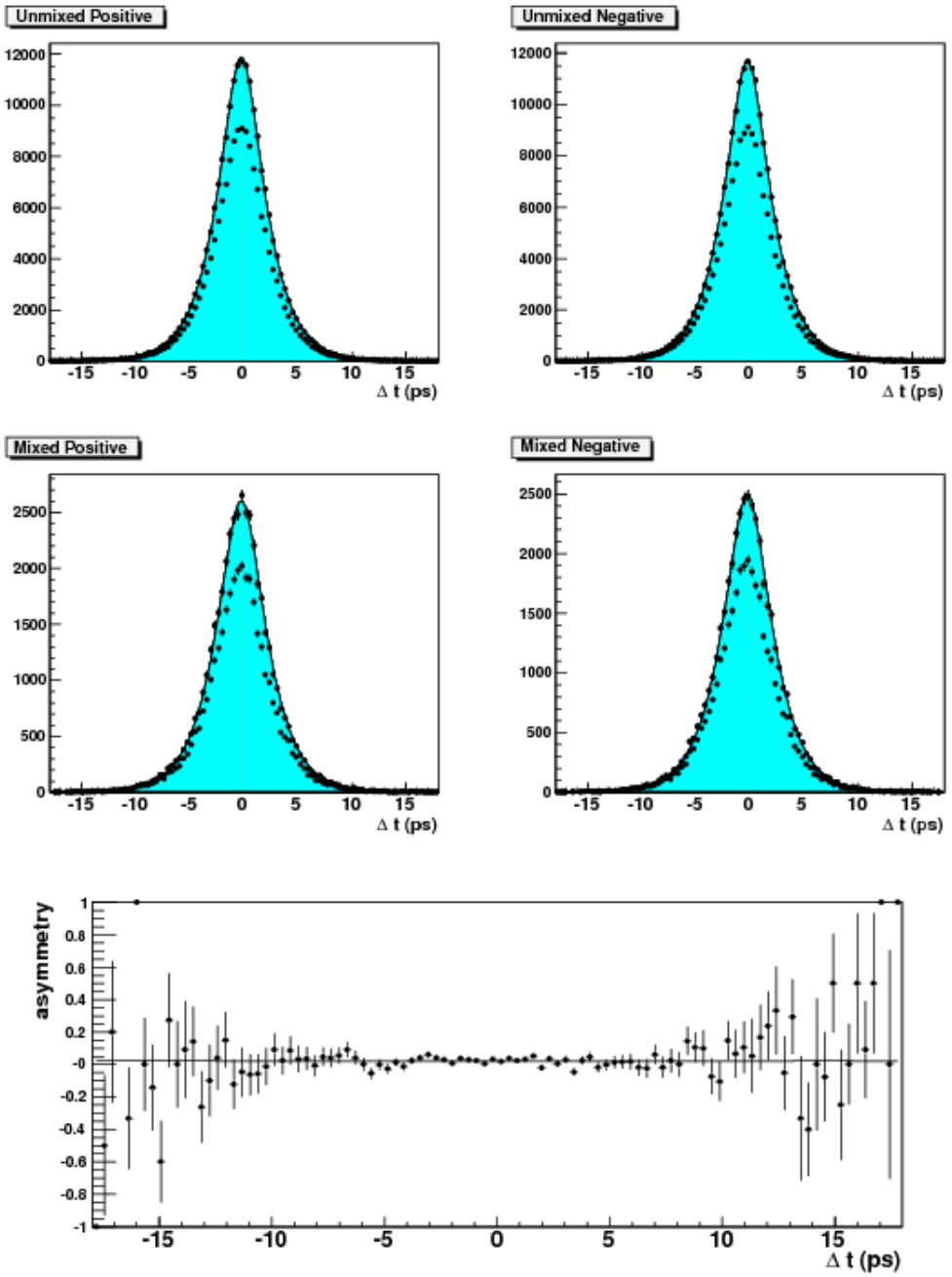

Figure 26: Fitted distributions for $B^0\overline{B}^0$ peaking B_{tag} events.

Table 12: Results of the fit to CP-eigenstates.

Parameter	Fit result
C_{eff}	-0.0619 ± 0.0147
S_{eff}	-0.0367 ± 0.0041

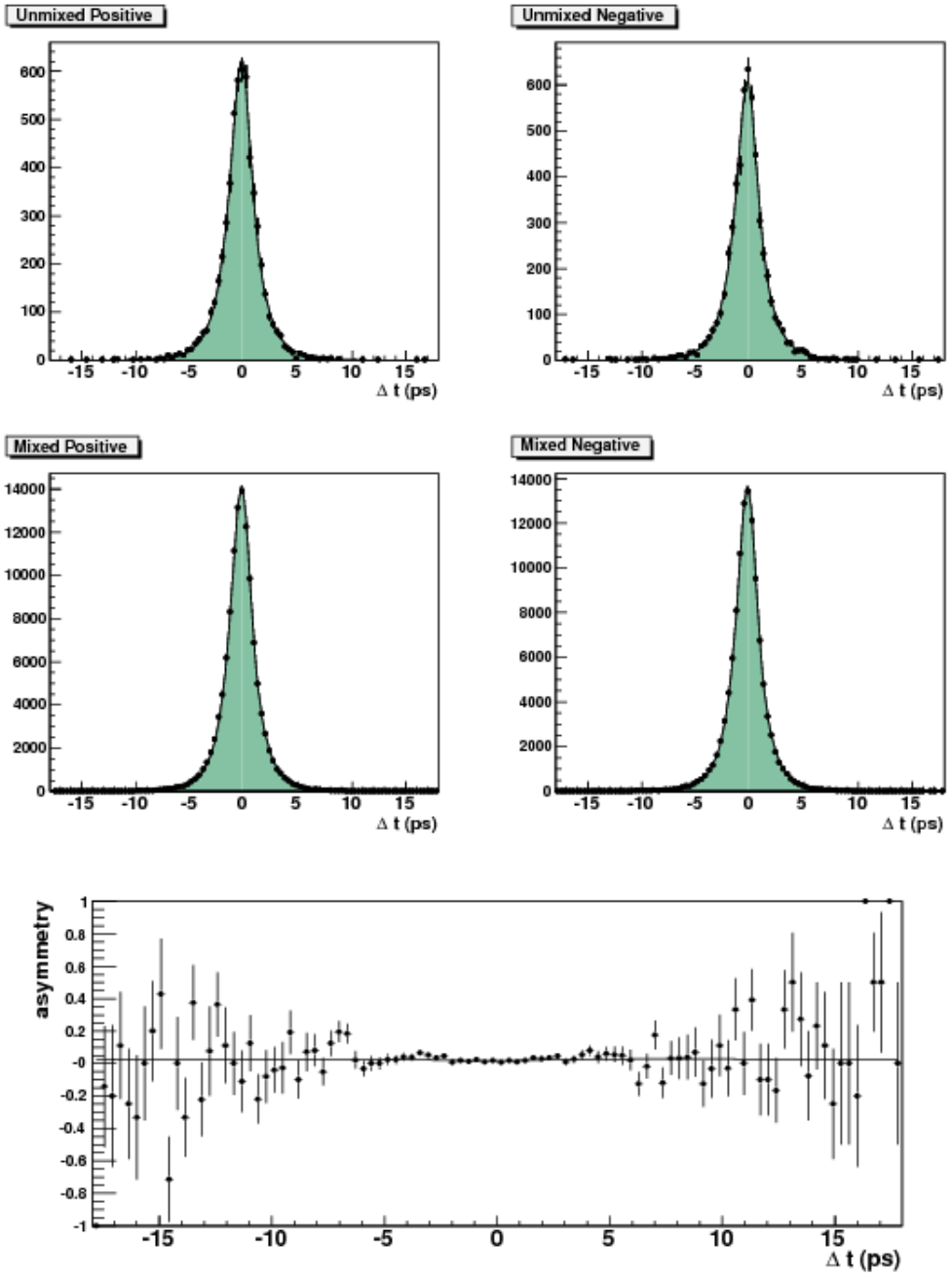

Figure 27: Distributions for the four samples (top plots) of peaking D_{tag} events with overlayed the fitting function found for the signal D_{tag} sample.

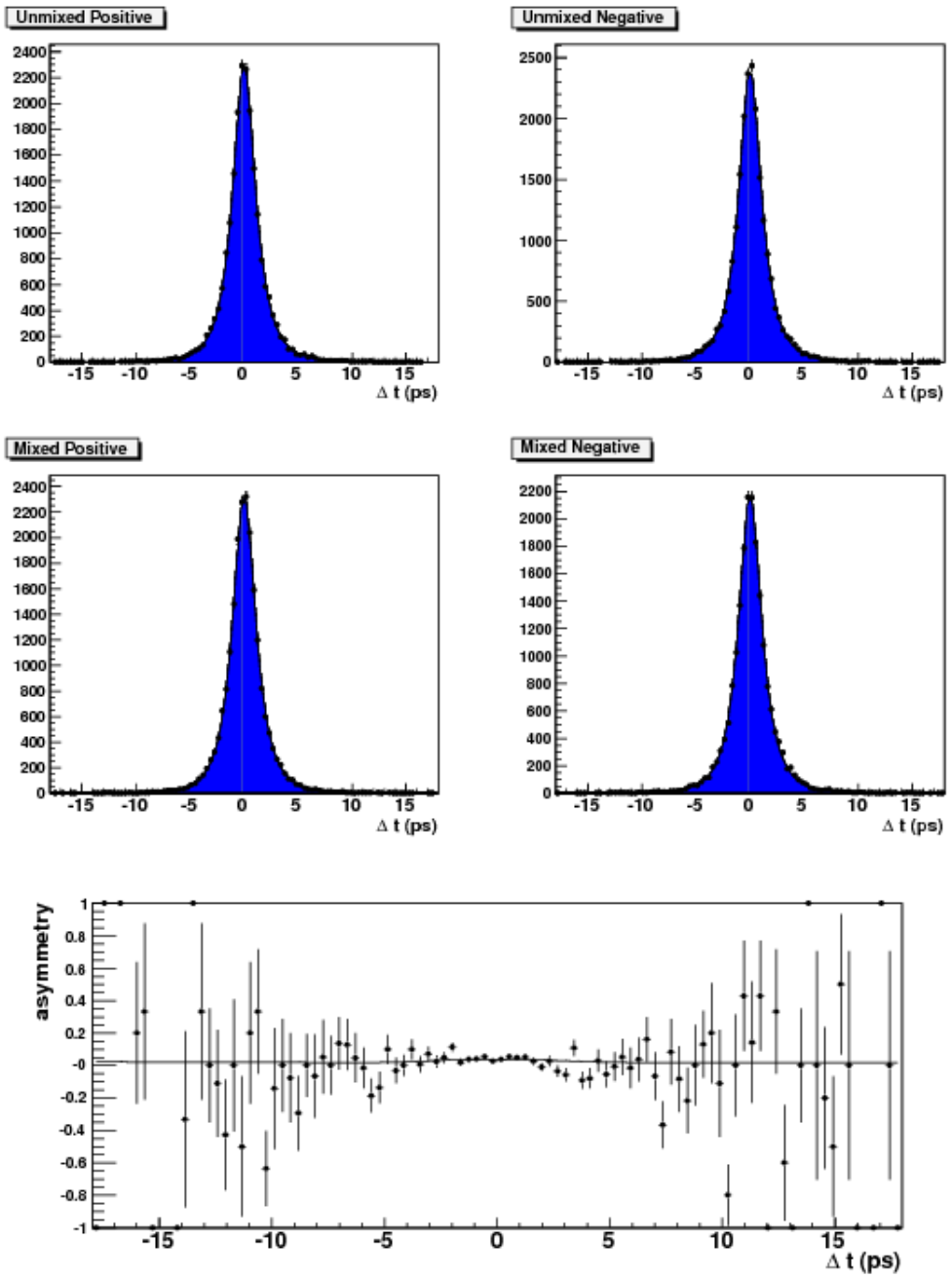

Figure 28: Fitted distributions for the four samples and the asymmetry for off-peak events.

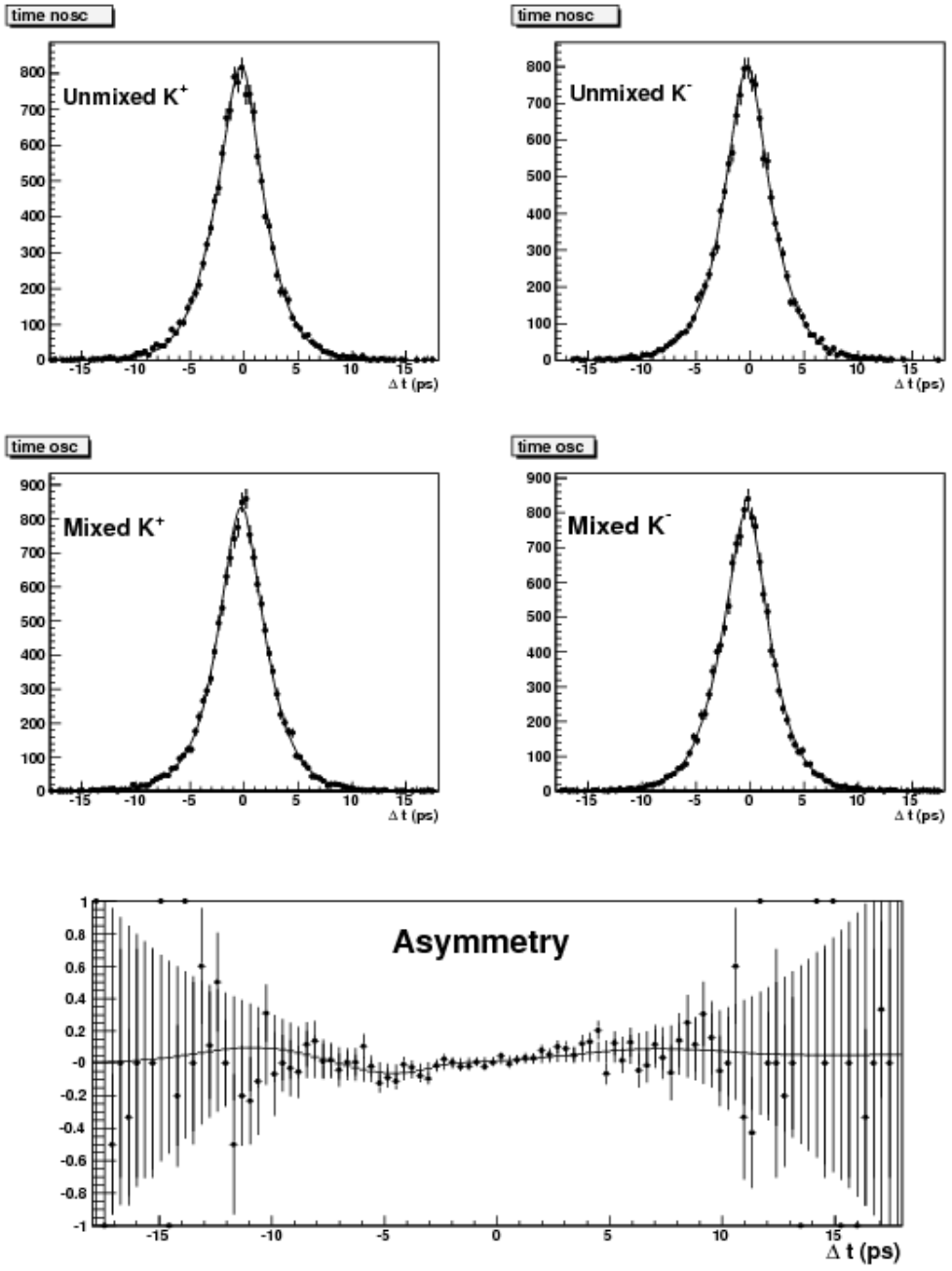

Figure 29: Fitted distributions for the four samples and the asymmetry for CP-eigenstates.

6.10 Test on Fitted Asymmetries

We validate the test on charge asymmetries performed on section 4.2, by comparing the fit results for $A_{rec}(e)$, $A_{rec}(\mu)$ and A_{tag} obtained by separately fitting each of the eight Monte Carlo samples.

Results are shown in figures 30 and 31. The agreement we find for every sample is impressively good, with deviations with respect to the average well within 2.5 σ.

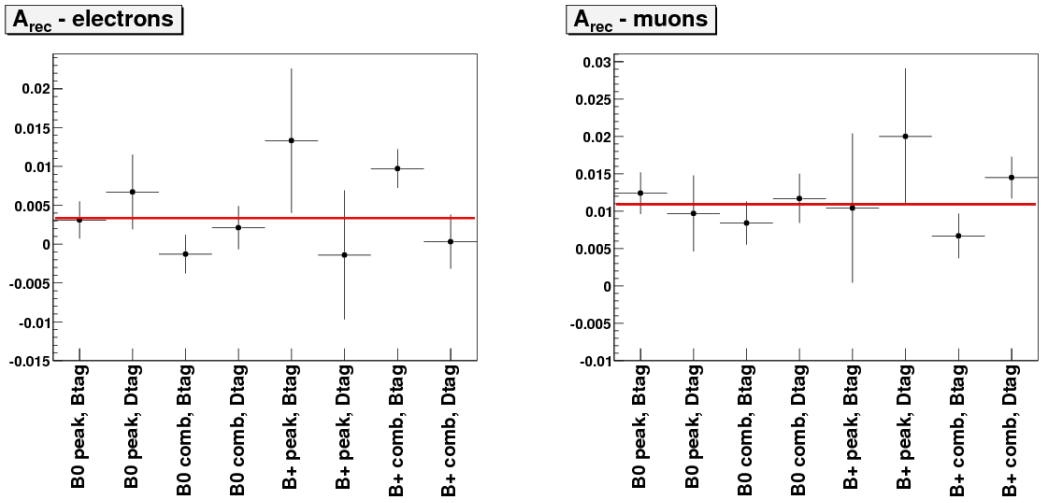

Figure 30: Reconstruction asymmetries $A_{rec}(e)$ (left plot) and $A_{rec}(\mu)$ (right) for the 8 Monte Carlo samples. The red line represents the weighted average of the asymmetries.

7 Validation on Toy Monte Carlo

Given the very large number of events we select in our analysis, it is not possible to generate signal Monte Carlo samples of adequate size. The validation of the fitting technique therefore proceeds on Toy Monte Carlo generated data samples.

7.1 Continuum

Monte Carlo samples of continuum events are generated from real off-peak data events according to the procedure which is explained in the following.

For each event, we consider the variables: $|\vec{p}_K|$, Δt, $\cos(\theta_{K\ell})$ and m_ν^2. For each of the above variables x_i, we define a gaussian pdf $G_i(x_i, \sigma_i)$, with mean value x_i and width σ_i. The value of σ_i is fixed for every event and is chosen empirically as the bin width of a histogram where the statistical fluctuations of x_i become evident. Each $G_i(x_i, \sigma_i)$ is used to generate the variable x_i'.

With this procedure, the generated event, with variables $(|\vec{p}_K|', \Delta t', \cos(\theta_{K\ell})', m_\nu^{2\prime})$, is *close* to the original one in the 4-dimensional parameter space and the correlations between the variables are preserved.

Figure 32 shows the comparison between the original distributions got from *off-peak* data events and the generated ones for the four variables of interest.

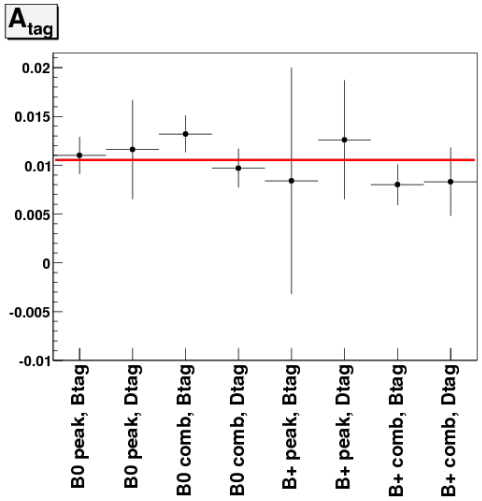

Figure 31: Reconstruction asymmetries A_{tag} for the 8 Monte Carlo samples. The red line represents the weighted average of the asymmetries.

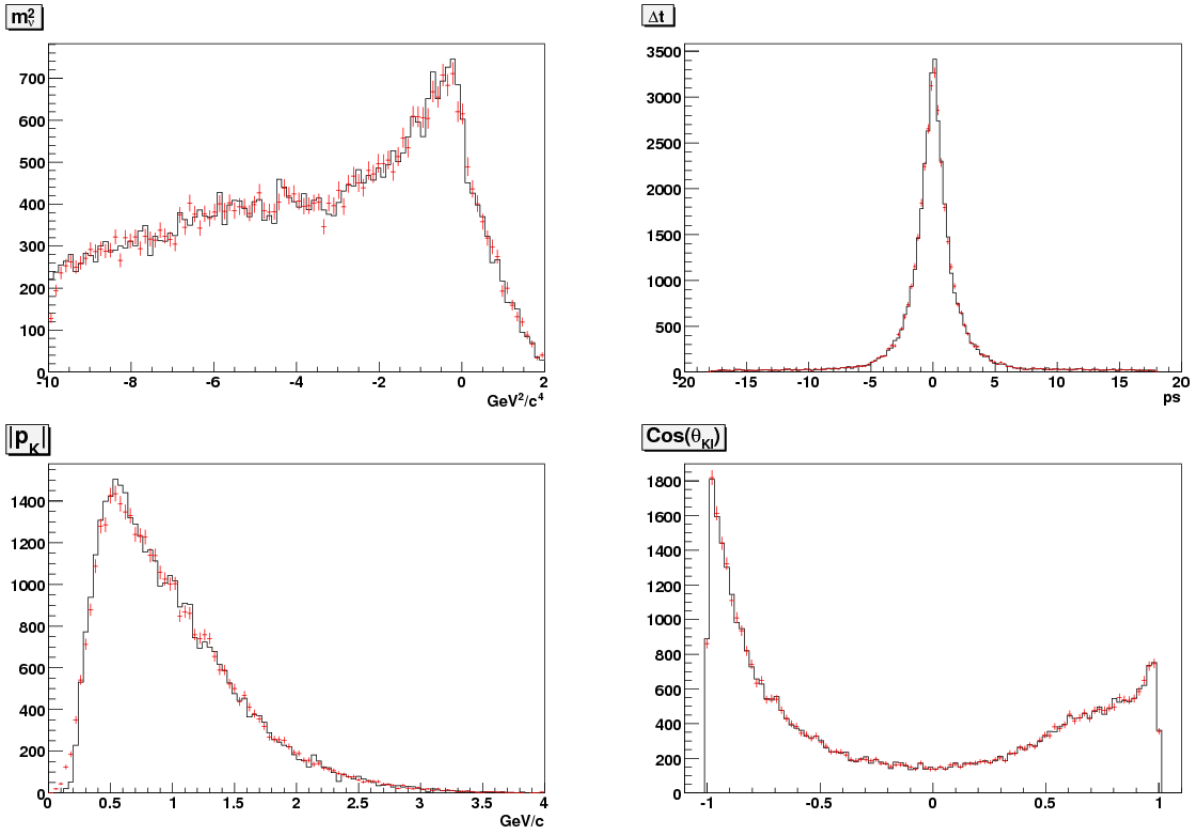

Figure 32: Original *off-peak* distributions (histograms) and modified ones (data points) for m_ν^2 (top left plot), Δt (top right), $|\vec{p}_K|$ (bottom left) and $\cos(\theta_{K\ell})$ (bottom right).

7.2 Toy MC with non-zero CP-violating parameters

We generate several samples of Monte Carlo events with non-zero CP-violating parameters by selectively discarding events from the initial generic MC sample.

The probability of keeping a $B\overline{B}$ event with generated difference of decay times of the two B mesons Δt_{true} is computed from the ratio of the Δt pdf with non-zero CP-violating parameters with the original one ($|q/p| = 1$, $b = c = 0$). In order to avoid the divergences which arise where the original pdf is zero and the modified one is not, we compute the ratio of the integrals of the two pdf's in 0.5 ps wide bins (significantly smaller than our resolution in Δt).

8 Validation on exclusively reconstructed $B^0 \to D^{*-}\ell^+\nu$ events

In this section, we will use a high purity sample of exclusively reconstructed $B^0 \to D^{*-}\ell^+\nu$ events to test on data the modeling of D_{tag} events.

8.1 Selection of $B^0 \to D^{*-}\ell^+\nu$ events

A subsample of exlusively reconstructed $B^0 \to D^{*-}\ell^+\nu$ events can be selected inside our sample of B_{rec} mesons by reconstructing the $\bar{D}^0$ decaying into the final states $K^+\pi^-$, $K^+\pi^-\pi^0$ and $K^+\pi^-\pi^+\pi^-$.

The candidate K is requested to pass the same `LooseKaonMicro` PID selector used for the standard selection of the main sample and to have opposite charge with respect to the π_{soft}. The mass of the D^* candidate has to satisfy the cut $2.008 < m_{D^*} < 2.012$ GeV/c^2 and the probability of the charged D^0 daughters to originate from a common vertex must exceed 1 %. A mode dependent cut on the mass of the D^0 candidate is applied: $1.845 < m_{D^0} < 1.880$ GeV/c^2 ($K\pi$), $1.850 < m_{D^0} < 1.880$ GeV/c^2 ($K\pi\pi^0$) and $1.855 < m_{D^0} < 1.875$ GeV/c^2 ($K3\pi$).

As in the partial reconstruction case, we compute m_ν^2 using equation (12). Given that in this case the D^* is fully reconstructed, the resolution on m_ν^2 is considerably better. We do not apply any cut on m_ν^2.

Kaon tracks originating from the D^0 decay are treated in the same way of candidate tag K tracks in the main sample; the variables Δt, $\sigma(\Delta t)$ and $\cos(\theta_{K\ell})$ are computed in the same way.

Figure 33 shows the m_ν^2 and Δt distributions for the selected events in generic $B^0\overline{B}^0$ Monte Carlo; the contribution from background is of the order of a few percent in all the three samples.

References

[1] M. Ciuchini et al. *Lifetime Differences and CP Violation Parameters of Neutral B Mesons*, JHEP 0308, 031 (2003).

[2] S. Laplace et al. *Implications of the CP asymmetry in semileptonic B decay*, Phys. Rev. D **65**, 094040 (2002).

[3] E. Nakano et al. *Charge Asymmetry of Same-Sign Dileptons in B^0-$\overline{B}^0$ Mixing*, Phys. Rev. D. **73**, 112002 (2006).

[4] B. Aubert et al. *Search for CPT and Lorentz violation in B^0-$\overline{B}^0$ oscillations with inclusive dilepton events*, Phys. Rev. Lett. **96**, 251802 (2006).

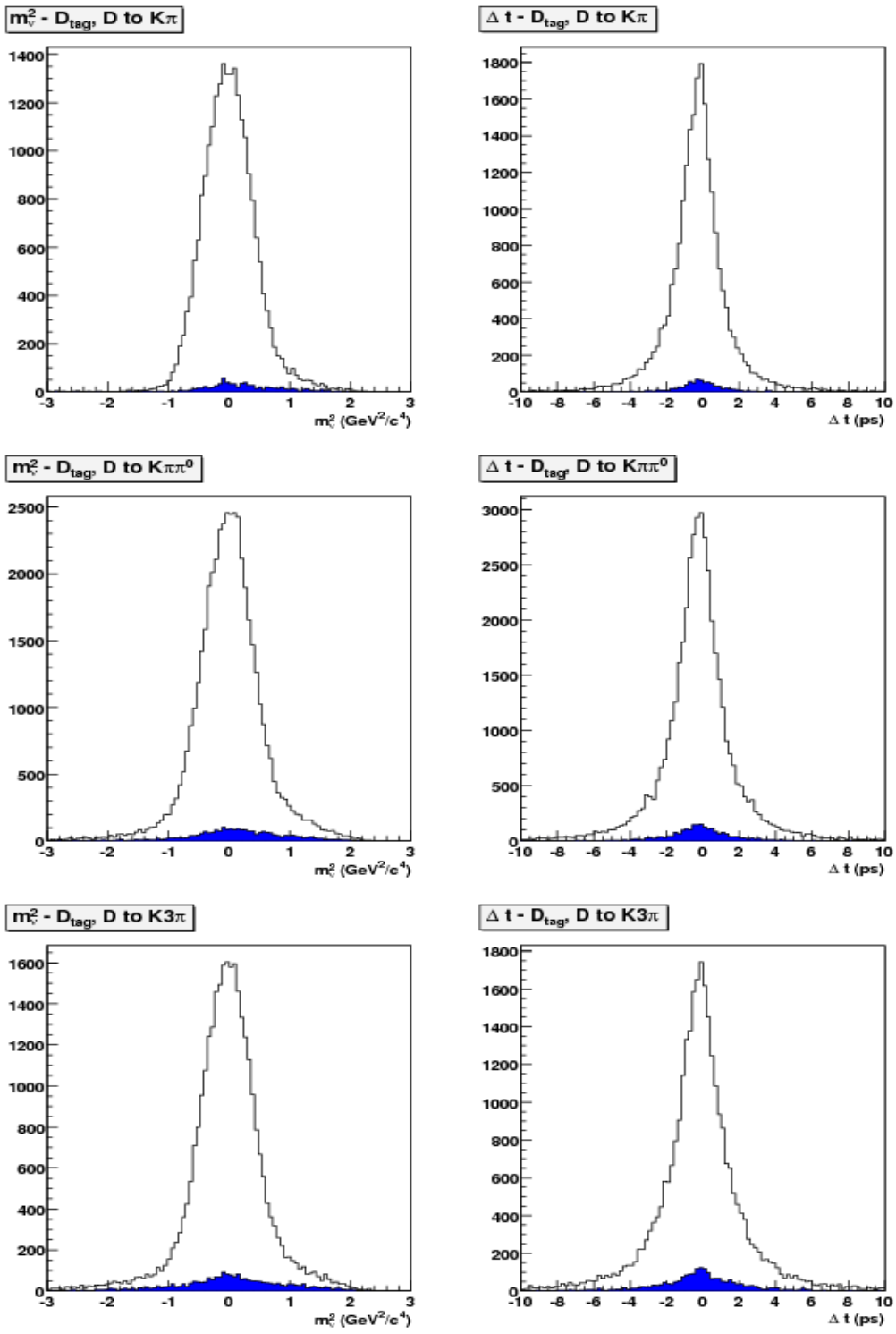

Figure 33: m_ν^2 (left plots) and Δt (right) distributions for exclusively reconstructed $B^0 \to D^{*-}\ell^+\nu$ events with $D^0 \to K\pi$ (top plots), $D^0 \to K\pi\pi^0$ (middle) and $D^0 \to K3\pi$ (bottom) for generic $B^0\overline{B}^0$ MC. The background contribution is shown in blue.

[5] V.M. Abazov et al. *Measurement of the CP-violation parameter of B^0 mixing and decay with $p\bar{p} \to \mu\mu X$ data*, Phys. Rev. D. **74**, 092001 (2006).

[6] R. Covarelli et al. *Measurement of CP violation in $B^0\overline{B}^0$ mixing using partially reconstructed $D^*\ell\nu$ events*, BAD 1168.

[7] O. Long et al. *Impact of tag-side interference on time-dependent CP asymmetry measurements using coherent $B^0\overline{B}^0$ pairs*, Phys. Rev. D **68** 034010 (2003).

[8] B. Aubert et al. *Limits on the Decay-Rate Difference of Neutral-B Mesons and on CP, T, and CPT Violation in $B^0\overline{B}^0$ Oscillations*, Phys. Rev. D **70**, 012007 (2004).

[9] F. Simonetto et al. *Partially reconstructed $\overline{B}^0 \to D^{*+}\ell^-\bar{\nu}_\ell$ decays*, BAD 1377.

[10] I. Narsky *StatPatternRecognition: A C++ Package for Statistical Analysis of High Energy Physics Data*, physics/0507143, 2005.

[11] I. Narsky *Optimization of Signal Significance by Bagging Decision Trees*, physics/0507157, 2005.